Longitudinal Stability of Twin-Fuselage Aircraft with Oscillations Due to Unattached Tails

by

Ryan K Spiller

A Thesis Presented in Partial Fulfillment
of the Requirements for the Degree
Master of Science

Approved April 2017 by the
Graduate Supervisory Committee:

Valana Wells, Chair
Frederick Garrett
Anoop Grewal

ARIZONA STATE UNIVERSITY

August 2017

ABSTRACT

This thesis describes a longitudinal dynamic analysis of a large, twin-fuselage aircraft that is connected solely by the main wing with two tails unattached by a horizontal stabilizer. The goal of the analysis is to predict the aircraft's behavior in various flight conditions. Starting with simple force diagrams of the longitudinal directions, six equations of motion are derived: three equations defining the left fuselage's motion and three equations defining the right fuselage's motion. The derivation uses a state-vector approach. Linearization of the system utilizes a Taylor series expansion about different trim points to analyze the aircraft for small disturbances about the equilibrium. The state transition matrix shows that there is a coupling effect from the reactionary moments caused by the two empennages through the connection of the main wing. By analyzing the system in multiple flight conditions: take-off, climb, cruise, and post-separation of payload, a general flight envelope can be developed which will give insight as to how the aircraft will behave and the overall controllability of the aircraft. The four flight conditions are tested with published Boeing 747 data confirmed from multiple sources. All four flight conditions contain unstable phugoid modes that imply instability increases with decreasing torsional spring stiffness of the wing or as the structural damping drops below 4%.

This thesis is dedicated to my loving family who has relentlessly supported me in my endeavors. Through all aspects of life, you have helped me fly.

ACKNOWLEDGMENTS

I would like to thank Dr. Valana Wells for chairing my committee and the opportunity to work with her as well as her guidance throughout the course of this thesis.

I also would like to thank Dr. Fred Garrett for his continued support and help in the culmination of this thesis – without his direction the creation of this thesis would not have been possible.

Finally, I would like to thank Dr. Mike Jeffries for voluntarily spending time to lend his insight and expertise in the stability analysis of this thesis.

TABLE OF CONTENTS

Page

LIST OF TABLES

Table Page

LIST OF FIGURES

Figure Page

NOMENCLATURE

i	=	body frame of reference forward direction
j	=	body frame of reference lateral direction
k	=	body frame of reference vertical direction
x	=	inertial frame of reference forward direction
y	=	inertial frame of reference lateral direction
z	=	inertial frame of reference vertical direction
α_l	=	left-body angle of attack
α_r	=	right-body angle of attack
α_{t_l}	=	left-body tail angle of attack
α_{t_r}	=	right-body tail angle of attack
M_w	=	total wing moment
L_w	=	total lift from wing
D_w	=	total drag from wing
L_t	=	total lift from tail
D_t	=	total drag from tail
m	=	mass
g	=	gravity
T_l	=	thrust from left-body
T_r	=	thrust from right-body

u	=	forward component velocity of aircraft
v	=	lateral component velocity of aircraft
w	=	vertical component velocity of aircraft
q_l	=	pitch rate of left-body
q_r	=	pitch rate of right-body
p	=	roll rate
r	=	yaw rate
V_l	=	magnitude velocity of left-body
V_r	=	magnitude velocity of right-body
S_{ref}	=	wing reference area
$S_{t_{ref}}$	=	tail reference area
ρ	=	density
$C_{l_{o_l}}$	=	left-body zero incidence lift coefficient
$C_{l_{o_r}}$	=	right-body zero incidence lift coefficient
$C_{d_{o_l}}$	=	left-body zero lift drag coefficient
$C_{d_{o_r}}$	=	right-body zero lift drag coefficient
$C_{l_{t_{o_l}}}$	=	left-tail zero incidence lift coefficient
$C_{l_{t_{o_r}}}$	=	right-tail zero incidence lift coefficient
$C_{d_{t_{o_l}}}$	=	left-tail zero lift drag coefficient

$C_{d_{t_{o_r}}}$ = right-tail zero lift drag coefficient

$C_{l_{a_l}}$ = left-body lift due to angle of attack

$C_{l_{a_r}}$ = right-body lift due to angle of attack

$C_{l_{t_{a_l}}}$ = left-tail lift due to angle of attack

$C_{l_{t_{a_r}}}$ = right-tail lift due to angle of attack

I_{yy} = lateral moment of inertia

k = induced drag coefficient

$\bar{c}$ = average chord of the wing

θ_l = left-body pitch angle

θ_r = right-body pitch angle

$C_{m_{o_l}}$ = left-body zero lift moment coefficient

$C_{m_{o_r}}$ = right-body zero lift moment coefficient

$C_{m_{q_l}}$ = left-body pitching moment coefficient

$C_{m_{q_r}}$ = right-body pitching moment coefficient

$C_{m_{a_l}}$ = left-body moment coefficient due to angle of attack

$C_{m_{a_r}}$ = right-body moment coefficient due to angle of attack

x_1 = static-margin distance

x_2 = moment arm between tail lift and center of gravity

ϵ = Young's modulus

I_{xy} = cross-sectional moment of inertia

K_{τ} = torsional spring constant

1. INTRODUCTION

1.1 New Frontiers

The advancements made in the aerospace field have been on par with the exponential growth of technology in the last century. From the Wright brothers recording the first manned flight in 1903, to landing on the moon in 1969, the aerospace industry has had an explosive growth rate. Flight went from being an illustrious dream to an everyday commodity in less than a lifetime. It seems fit that aerospace is now tackling the next frontier in space; technological advancements have made space increasingly accessible every year – just like with planes before in the sky. However, the debate on the most practical, efficient, and reliable method to reach space still battles on within the industrial and academic fields.

1.2 Reusable Air-Breathing First Stage Approach

One method that has emerged within the last few decades is the air-launched rocket approach. Essentially, a carrier aircraft takes a rocket or spacecraft into the atmosphere, generally the stratosphere, where the rocket or spacecraft is detached from the carrier and begins its self-powered flight. This approach, like any other, offers its set of benefits and cons when compared to the more conventional method of launching from the ground. Even within this new tactic of air-launched vehicles, there is still debate on the most efficient method of carrying the payload into the stratosphere. Recently, twin-fuselage designed aircraft have had somewhat of a revival from when they were used in World War II as long-distance bombers, escorts, and fighter planes. Aircraft like the F-82 Twin Mustang existed because military efforts demanded new aircraft with more capability with the resources available and very limited design time; it was simply easier to increase the range

by combining two aircraft into one rather than make a completely new, clean-sheet design.

However, the design has made a comeback with aircraft like the White Knight Two from Virgin Galactic and the Stratolaunch M351 from Scaled Composites and Vulcan Aerospace. Both aircraft were designed to carry a rocket or spacecraft to high altitudes to perform mid-air launches. The White Knight Two has already flown successfully while the considerably larger Stratolaunch air-carrier is currently in development. White Knight Two has already flown successfully, but the question posed here is can the design model retain its effectiveness with an aircraft the size of the Stratolaunch M351 which will have the largest wingspan of any constructed aircraft in history.

1.3 Literature Review

Previously, numerical model simulators and test flight simulations have been performed to study the flight dynamics of large twin-fuselage aircraft with unattached tails. Two tests, done by NASA Langley in the 1980's, were performed on similar concepts to look at flight characteristics and pilot response.

In 1983, the NASA technical report "Simulator Study of Flight Characteristics of a Large Twin-Fuselage Cargo Transport Airplane during Approach and Landing" utilized a six-degree of freedom simulation study to analyze low-speed flight characteristics of a twin-fuselage cargo transport aircraft. One of the primary results of the study provided pilot ratings and feedback on the longitudinal and lateral-directional characteristics. Longitudinally, the pilots rated the aircraft "feel" in pitch response and handling qualities as "acceptable" but "sluggish" in pitch response specifically (Grantham 11). Lateral-directionally, the pilot rating was poor. The reasoning for the low rating was due to the

"large adverse sideslip experienced during rolling maneuvers" (Grantham 12). Overall, the longitudinal handling qualities of the twin-fuselage aircraft received a pilot rating of "acceptable, but unsatisfactory" and lateral-directional handling qualities received an "uncontrollable" rating (Grantham 21).

In 1984, the NASA contractor report "An In-Flight Investigation of a Twin Fuselage Configuration in Approach and Landing" looked at the handling and ride qualities of a twin-fuselage aircraft in the USAF-AFWAL Total In-Flight Simulator. Similar to the 1983 report, the lateral-directional handling qualities were unsatisfactory due to high roll modes. The 1983 report primarily focused on looking at high sideslip angles caused by rolling maneuvers, and somewhat looked piloting position during landing; the 1984 report looked at how the pilot-rated handling qualities changed with respect to the offset cockpit position. The study concluded "lateral pilot position has a significant effect on pilot ratings and comments during landing approach and touchdown" (Weingarten, 4-32). With the large pilot offsets from the aircraft's centerline and fast roll mode times, the aircraft experienced a coupling of roll and pitch oscillations that the pilots tried to correct but may have exasperated with input lag. The paper went on to define a potential limit of pilot offset that will cause handling quality deterioration. Both papers from NASA Langley described pilot-rated flight qualities and characteristics of potential large, twin-fuselage aircraft, and both studies generated difficult flight conditions for the pilots to overcome. This continues to raise the question of the feasibility of twin-fuselage carrier aircraft the size of the Stratolaunch M351.

1.4 The Stratolaunch

Vulcan Aerospace presented the Stratolaunch air–launch platform as a potential means to reduce the cost and increase the availability of low Earth orbits as a commercial enterprise.

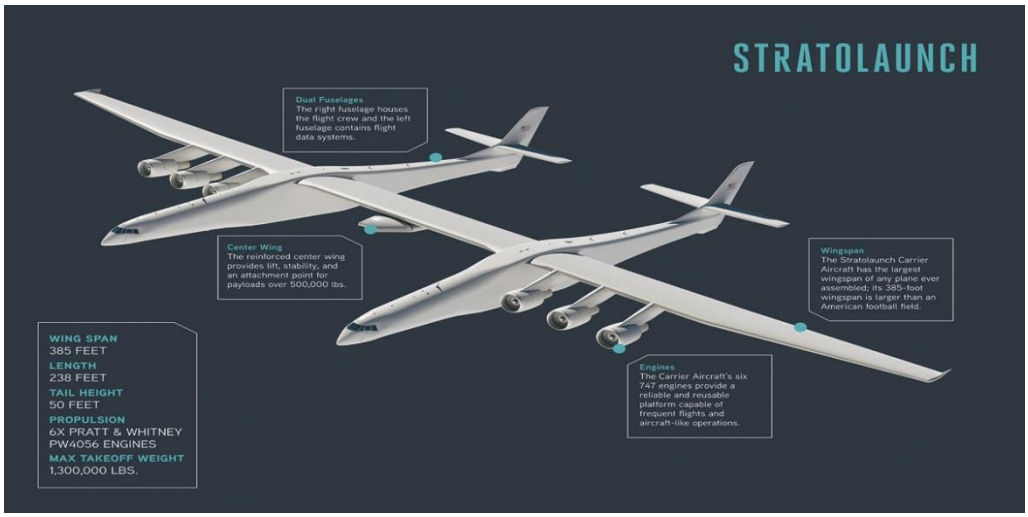

Fig 1.1 Stratolaunch Aircraft with Physical Dimensions.

The aircraft deemed the M351 from the manufacturer Scaled Composites is comprised of two modified Boeing 747 fuselages made of carbon fiber composite attached together by a new wing and powered by six Pratt & Whitney PW4056 engines. With the intention of launching heavy payloads while in flight, the Stratolaunch air carrier faces considerable challenges – specifically with concerns about the aircraft's stability and controllability. Precedence from previous, and smaller, twin-empennage aircraft have usually connected the two tails together with a longer horizontal stabilizer; however, the Stratolaunch has elected to leave the twin empennages unattached like the White Knight Two. Leaving the two tails unconnected leads to questions regarding how the aircraft will react in different flight conditions. Essentially, the aircraft can be viewed

as a wing acting like a torsional spring with two extended bodies attached; the wing acts as the spring and the two fuselages act as the extended bodies. Without anything connecting the two tails, there is the potential for the tails to have an unstable mode operating on different frequencies in the longitudinal plane or diverging apart completely. The only damping acting on the tails is the structural damping from the composite wing. Since there is no horizontal stabilizer connecting the two tails, there will be a coupling effect from the reactionary moments on each body in flight. In this thesis, it will be attempted to accurately model the Stratolaunch aircraft in the longitudinal plane with the moment coupling between the left and right fuselages and to analyze the stability at four different equilibriums points corresponding to different flight conditions: take-off, climb, cruise, and the orientation after the initial release of the payload mid-flight.

2. DEVELOPMENT

2.1 Stratolaunch Model

Since the question in hand is at its core an analysis of the longitudinal stability of the aircraft, the initial framework of the problem can be viewed as a typical stability problem. Free-body diagrams for the left and right fuselages of the aircraft in flight were found using the known acting forces on the aircraft with respect to the aircraft's neutral point centered in between the two fuselages. The free-body diagrams were created in the body reference plane of the aircraft in order to focus on the forces acting in flight; however, this reference plane would need to be changed to the inertial reference frame later to continue the analysis which will be discussed further in the development.

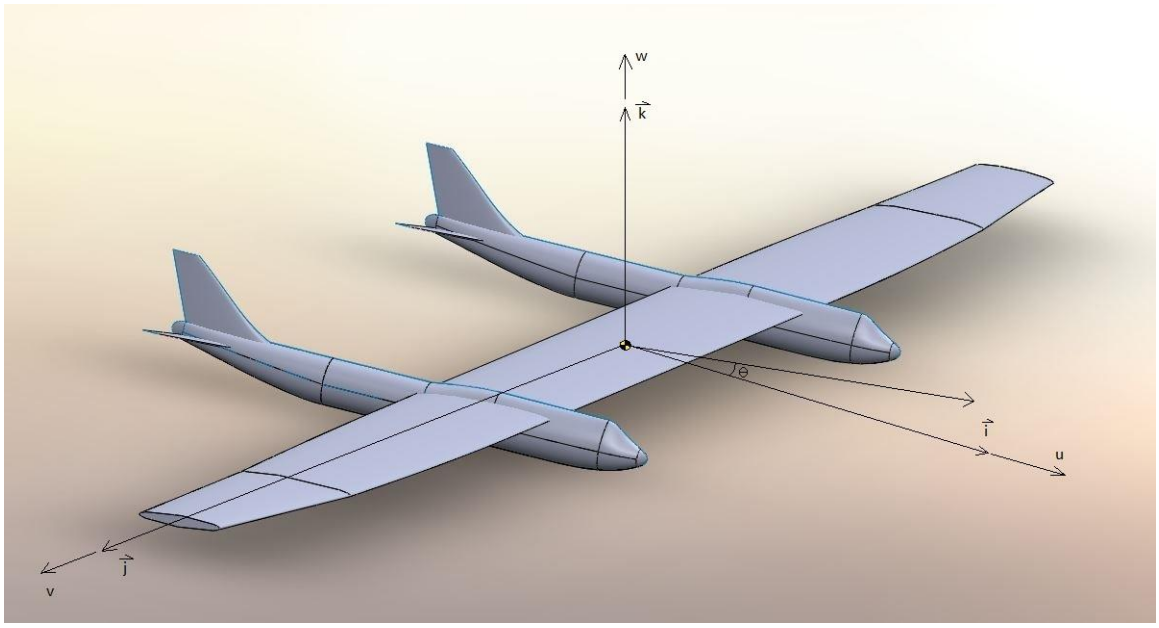

Fig. 2.1 Body frame of reference for the model aircraft.

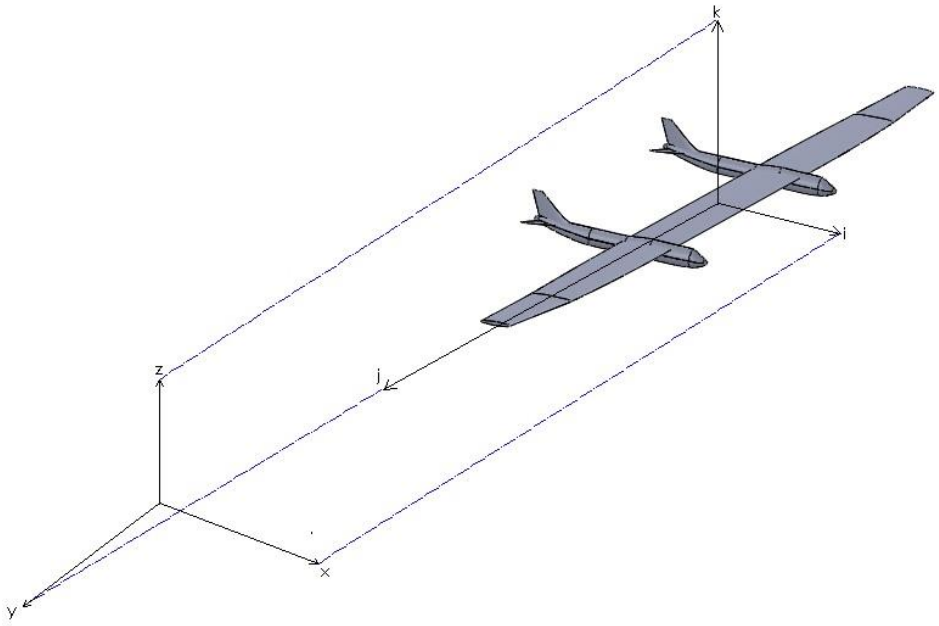

Fig. 2.2 Inertial & Body Reference Frame

2.2 Free Body Diagram

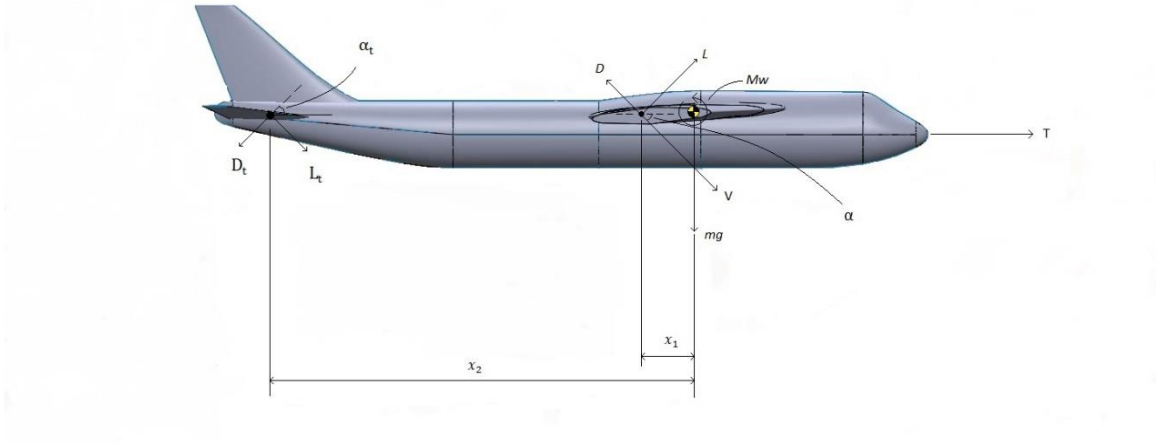

Fig. 2.3 Free-body diagram for the right fuselage. (Left fuselage is a mirrored free body diagram)

The free-body diagrams for each body included their respective forces due to lift and drag from both the main wing and the tail, the force due to engine thrust from their relative side of the neutral point, the weight of each body, and the moments about the neutral point.

2.3 Forces in Flight

The lift forces were composed of the lift at zero-degree angle of attack and the lift due to a change in angle of attack.

$$L = \frac{1}{2}\rho V^2 S_{ref} C_L$$

Where

$$C_L = C_{L_o} + C_{L_\alpha} \quad (1)$$

Similarly, the drag forces were composed the drag at zero lift and the induced drag due to lift– also known as the drag polar.

$$D = \frac{1}{2}\rho V^2 S_{ref} C_D$$

Where

$$C_D = C_{D_o} + KC_L^2 \quad (2)$$

As stated before, the moments were taken about the neutral point of the aircraft. Aerodynamic forces from both the main wing and tail caused moments; however, even though the thrust-line does not perfectly intersect the center of gravity, the distance is small enough to have a negligible effect on the outcome of the analysis. The reactionary moments that were the point of focus in the model came from the two fuselage bodies moving at different angles. Effectively, the wing connecting the two bodies acted as a torsional spring within its elastic bounds, so each body caused a reactionary moment in the other. The value of the moment was modeled from the difference in pitch angle

between the two bodies multiplied by a torsional spring constant. These reactionary moments caused there to be a coupling between the dynamics of the two bodies which will be discussed further in the analysis.

$$M = K_S(\theta_L - \theta_R)M_L + K_S(\theta_R - \theta_L)M_R \tag{3}$$

where $$M_L = \frac{1}{2}\rho V_L^2 C_{M_L} \bar{c}\, S_{\text{ref}}$$

and $$M_R = \frac{1}{2}\rho V_R^2 C_{M_R} \bar{c}\, S_{ref}$$

Furthermore, $$C_{M_L} = C_{M_{L_o}} + C_{M_{L_\alpha}}\alpha_L + C_{M_{L_q}} q_L$$

And $$C_{M_R} = C_{M_{R_o}} + C_{M_{R_\alpha}}\alpha_R + C_{M_{R_q}} q_R$$

So, $$M = \frac{1}{2}\rho \bar{c}\, S_{ref} K_S \left[V_L^2(\theta_L - \theta_R)\left(C_{M_{L_o}} + C_{M_{L_\alpha}}\alpha_L + C_{M_{L_q}} q_L\right) + V_R^2(\theta_R - \theta_L)\left(C_{M_{R_o}} + C_{M_{R_\alpha}}\alpha_R + C_{M_{R_q}} q_R\right)\right] \tag{4}$$

With the free-body diagrams, the next step was to sum the forces in the forward and vertical directions for the left and right bodies of the aircraft, and sum the moments about the neutral point of both bodies in the longitudinal plane.

$$\sum F_{L_i} = m_L \dot{u}_L = \frac{1}{2}\rho V_L^2 S_{ref}\left(C_{L_{o_L}} + C_{L_{\alpha_L}}\alpha_L\right)\sin(\alpha_L) - \frac{1}{2}\rho V_L^2 S_{ref}\left(C_{D_{o_L}} + K\left(C_{L_{o_L}} + C_{L_{\alpha_L}}\alpha_L\right)^2\right)\cos(\alpha_L) + \frac{1}{2}\rho V_L^2 S_{t_{ref}}\left(C_{L_{t_{o_L}}} + C_{L_{t_{\alpha_L}}}\alpha_{t_L}\right)\sin(\alpha_{t_L}) - \frac{1}{2}\rho V_L^2 S_{t_{ref}}\left(C_{D_{T_{o_L}}} + K\left(C_{L_{t_{o_L}}} + C_{L_{t_{\alpha_L}}}\alpha_{t_L}\right)^2\right)\cos(\alpha_{t_L}) + T\cos(\theta_L) \tag{5}$$

$$\sum F_{L_k} = m_{_L}\, \dot{w}_L \tag{6}$$

$$= \frac{1}{2}\rho V_L^2 S_{ref}\left(C_{L_{o_L}} + C_{L_{\alpha_L}}\alpha_L\right)\cos(\alpha_L)$$

$$+ \frac{1}{2}\rho V_L^2 S_{ref}\left(C_{D_{o_L}} + K\left(C_{L_{o_L}} + C_{L_{\alpha_L}}\alpha_L\right)^2\right)\sin(\alpha_L)$$

$$- \frac{1}{2}\rho V_L^2 S_{t_{ref}}\left(C_{L_{t_{o_L}}} + C_{L_{t_{\alpha_L}}}\alpha_{t_L}\right)\cos(\alpha_{t_L})$$

$$- \frac{1}{2}\rho V_L^2 S_{t_{ref}}\left(C_{D_{t_{o_L}}} + K\left(C_{L_{t_{o_L}}} + C_{L_{t_{\alpha_L}}}\alpha_{t_L}\right)^2\right)\sin(\alpha_{t_L}) + T\sin(\theta_L)$$

$$- m_L g$$

$$\sum M_{L_j} = I_{yy}\ddot{\theta} \tag{7}$$

$$= \frac{1}{2}\rho \bar{c}\, S_{ref} K_S\left[V_L^2(\theta_L - \theta_R)\left(C_{M_{L_o}} + C_{M_{L_\alpha}}\alpha_L + C_{M_{L_q}}q_L\right)\right.$$

$$\left. + V_R^2(\theta_R - \theta_L)\left(C_{M_{R_o}} + C_{M_{R_\alpha}}\alpha_R + C_{M_{R_q}}q_R\right)\right]$$

$$+ \frac{1}{2}\rho V_L^2 S_{t_{ref}}\left[\left(C_{L_{t_{o_L}}} + C_{L_{t_{\alpha_L}}}\alpha_{t_L}\right)\cos(\alpha_{t_L})\right.$$

$$\left. + \left(C_{D_{t_{o_L}}} + K\left(C_{L_{t_{o_L}}} + C_{L_{t_{\alpha_L}}}\alpha_{t_L}\right)^2\right)\sin(\alpha_{t_L})\right]x_2 - m_L g x_1$$

The equations of motion representing the right body are mirrored equations from the left.

Since the acceleration in the j-direction ($\dot{v}$) was assumed to be negligibly small to focus on the longitudinal stability, the sum of the forces in the j-direction of the aircraft were zero. With these sums of forces, the equations of motion for the aircraft in the

longitudinal plane were described; however, these sums could not accurately depict the motion of the aircraft because they were found in the body reference frame relative only the aircraft itself. In order to continue with the stability analysis, the equations of motion needed to be relative to an inertial reference frame where Newtonian physics was applicable. The equations in the body reference frame were translated to an inertial frame of reference connected to the Earth. Additionally, the Earth was assumed to be a flat and stationary reference point to simplify the equations of motion since the general stability of the aircraft would not change with that simplification.

To translate to an inertial reference frame, maneuver rates of the aircraft needed to be defined such that the roll rate (p) and yaw rate (r) were negligibly small, and the pitch (q) was equal the change in pitch angle in the body frame ($\dot{\theta}$).

$$p = \text{roll rate} = 0 \tag{8}$$

$$q = \dot{\theta} = \text{pitch rate} \neq 0 \tag{9}$$

$$r = \text{yaw rate} = 0 \tag{10}$$

The inertial frame of reference was equal to the body frame of reference plus the cross product between the maneuver rates and the body-directional velocities.

$$\left(\frac{\partial \vec{V}}{\partial t}\right)_i = \left(\frac{\partial \vec{V}}{\partial t}\right)_b + \vec{\omega}\, x\, \vec{V}$$

$$= \left(\frac{\partial u}{\partial t}\hat{\imath}_b + \frac{\partial v}{\partial t}\hat{\jmath}_b + \frac{\partial w}{\partial t}\hat{k}_b\right) + \begin{vmatrix} \hat{\imath}_b & \hat{\jmath}_b & \hat{k}_b \\ p & q & r \\ u & v & w \end{vmatrix} \tag{11}$$

Therefore, $$\sum F_x = m(\dot{u} + qw - rv) \tag{12}$$

$$\sum F_y = m(\dot{v} + ru - pw) \tag{13}$$

$$\sum F_z = m(\dot{w} + pv - qu\ ) \tag{14}$$

And from Eq. 8,9, & 10 above,

$$\sum F_x = m\dot{u} + mqw \tag{15}$$

$$\sum F_y = 0 \tag{16}$$

$$\sum F_z = m\dot{w} - mqu \tag{17}$$

The full equations of motion in the inertial frame of reference were found for inertial coordinate system based on previous calculations from Eq. 15, 16, and 17.

The translation between the body and inertial reference frame for the moment can be a much more tedious calculation; however, with the assumptions of negligible roll and yaw rate, the sum of the moments in the inertial reference frame were simply equal to the sum of moments in the body reference frame.

$$\left(\frac{\partial \vec{h}}{\partial t}\right)_i = \left(\frac{\partial \vec{h}}{\partial t}\right)_b + \vec{\omega}\ x\ \vec{h}$$

$$= \left(\frac{\partial h_x}{\partial t}\hat{\imath}_b + \frac{\partial h_y}{\partial t}\hat{\jmath}_b + \frac{\partial h_z}{\partial t}\hat{k}_b\right) + \begin{vmatrix} \hat{\imath}_b & \hat{\jmath}_b & \hat{k}_b \\ p & q & r \\ h_x & h_y & h_z \end{vmatrix} \tag{18}$$

Since $$\vec{h} = I\vec{w} = \begin{bmatrix} I_{xx} & -I_{xy} & -I_{xz} \\ -I_{xy} & I_{yy} & -I_{yz} \\ -I_{xz} & -I_{yz} & I_{zz} \end{bmatrix} \begin{bmatrix} p \\ q \\ r \end{bmatrix}$$

then

$$h_x = I_{xx}p - I_{xz}q - I_{xz}r \tag{19}$$

$$h_y = -I_{xy}p + I_{yy}q - I_{yz}r \tag{20}$$

$$h_z = -I_{xz}p - I_{yz}q + I_{zz}r \tag{21}$$

Since the analysis was done solely in the longitudinal plane, all the cross-coupled moments of inertia were negligible along with the roll and yaw rates.

$$h_x = 0 \tag{22}$$

$$h_y = I_{yy}q \tag{23}$$

$$h_z = 0 \tag{24}$$

Due to the analysis being done at specific instances of the flight, the mass was assumed to be unchanging.

$$\frac{\partial h_y}{\partial t} = I_{yy}\dot{q} = I_{yy}\ddot{\theta} \tag{25}$$

As it turned out, the inertial reference frame moment was equal to the body reference frame moment.

2.4 Frame of Reference Translation

At this moment, Newton's laws were valid with the aircraft's equations of moment in the inertial reference frame, but state variables needed to be defined to analyze the dynamics of the system. From the equations of motion, the most obvious set of state variables would be the forward velocity (x), vertical velocity (z), pitch angle (θ), and the pitch rate ($\dot{\theta}$); however, these variables did not best describe the more general and intuitive dynamics of the aircraft. Instead of using the component velocities, the vector of

the velocities' magnitude and the angle of attack better described the general dynamics of the system. Thus, a new state vector for both the left and right body was defined.

$$\begin{bmatrix} u \\ v \\ \theta \\ q \end{bmatrix} \rightarrow \begin{bmatrix} V \\ \alpha \\ \theta \\ q \end{bmatrix}$$

Transforming the state variables was a straight-forward process since the variables had a geometrical relationship found from the model of the aircraft.

$$V = \sqrt{u^2 + v^2 + w^2} \text{ where } v = 0 \text{ ,}$$

$$V = \sqrt{u^2 + w^2} \rightarrow V^2 = u^2 + w^2 \tag{26}$$

$$\frac{\partial V}{\partial t} V = \frac{\partial}{\partial t}(u^2 + w^2) \rightarrow 2V\dot{V} = 2u\dot{u} + 2w\dot{w}$$

$$\dot{V} = \frac{u}{V}\dot{u} + \frac{w}{V}\dot{w} = \frac{1}{V}(u\dot{u} + w\dot{w}) \tag{27}$$

And

$$\tan(\alpha) = \frac{w}{u} \tag{28}$$

$$\frac{\partial}{\partial t}\tan(\alpha) = \frac{\partial}{\partial t}\left(\frac{w}{u}\right) \rightarrow \dot{\alpha}\sec^2(\alpha) = \frac{u\dot{w} - w\dot{u}}{u^2}$$

$$\dot{\alpha} = \left(\frac{\dot{w}}{u} - \frac{\dot{u}w}{u^2}\right)\cos^2(\alpha) = \left(\frac{\dot{w}}{u} - \frac{\dot{u}}{u}\tan(\alpha)\right)\cos^2(\alpha)$$

$$\dot{\alpha} = \frac{\dot{w}}{u}\cos^2(\alpha) - \frac{\dot{u}}{u}\sin(\alpha)\cos(\alpha) \tag{29}$$

With the state vector in the more general form of (V) and (α), a set of non-linear equations of motion now defined the system. To simplify the system for the sake of analysis the equations were linearized using a Taylor series expansion. Two approaches

to the linearization were considered: the method of Taylor series expansion of the state variables, and a small-angle approximation. Either methods would have accomplished the same thing – linearizing the equations of motion for further analysis, but the Taylor series expansion was chosen due to the familiarity of the method within controls analysis and the ease of implication. The linearization constrained the range of values that could be analyzed for the system, so the analysis of the system would only be valid in a small area about the chosen equilibrium point.

Before the linearization, the previous inertially transformed state variables, $\dot{u}$ and $\dot{w}$, were substituted into the new state variables

$$\dot{u} = \frac{\sum F_x}{m} - qw$$

$$\dot{w} = \frac{\sum F_z}{m} + qu$$

Therefore, $\dot{V} = \frac{1}{V}\left(u\left(\frac{\sum F_x}{m} - qw\right) + w\left(\frac{\sum F_z}{m} + qu\right)\right)$

and, $\dot{\alpha} = \left(\frac{\sum F_z}{mu} + q\right)\cos^2(\alpha) - \left(\frac{\sum F_x}{mw} - q\right)\sin(\alpha)\cos(\alpha)$

$$\begin{bmatrix} \dot{V}_L \\ \dot{\alpha}_L \\ \dot{\theta}_L \\ \dot{q}_L \\ \dot{V}_R \\ \dot{\alpha}_R \\ \dot{\theta}_R \\ \dot{q}_R \end{bmatrix} = \begin{bmatrix} \frac{1}{V_L}\left(u_L\left(\frac{\sum F_{x_L}}{m_L} - q_L w_L\right) + w_L\left(\frac{\sum F_{z_L}}{m_L} + q_L u_L\right)\right) \\ \left(\frac{\sum F_{z_L}}{m_L\ u_L} + q_L\right)\cos^2(\alpha_L) - \left(\frac{\sum F_{x_L}}{m_L w_L} - q_L\right)\sin(\alpha_L)\cos(\alpha_L) \\ q_L \\ [\frac{1}{2}\rho \bar{c}\, S_{ref} K_S\left[V_L^2(\theta_L - \theta_R)\left(C_{M_{L_o}} + C_{M_{L_\alpha}}\alpha_L + C_{M_{L_q}} q_L\right) + V_R^2(\theta_R - \theta_L)\left(C_{M_{R_o}} + C_{M_{R_\alpha}}\alpha_R + C_{M_{R_q}} q_R\right)\right] + \\ \frac{1}{2}\rho V_L^2 S_{t_{ref}}\left[\left(C_{L_{t_{o_L}}} + C_{L_{t_{\alpha_L}}}\alpha_{t_L}\right)\cos(\alpha_{t_L}) + \left(C_{D_{t_{o_L}}} + K\left(C_{L_{t_{o_L}}} + C_{L_{t_{\alpha_L}}}\alpha_{t_L}\right)^2\right)\sin(\alpha_{t_L})\right] x_2 - m_L g x_1\ ] \\ \frac{1}{V_R}\left(u_R\left(\frac{\sum F_{x_R}}{m_R} - q_R w_R\right) + w_R\left(\frac{\sum F_{z_R}}{m_R} + q_R u_R\right)\right) \\ \left(\frac{\sum F_{z_R}}{m_R\ u_R} + q_R\right)\cos^2(\alpha_R) - \left(\frac{\sum F_{x_R}}{m_R w_R} - q_R\right)\sin(\alpha_R)\cos(\alpha_R) \\ q_R \\ [\frac{1}{2}\rho \bar{c}\, S_{ref} K_S\left[V_L^2(\theta_L - \theta_R)\left(C_{M_{L_o}} + C_{M_{L_\alpha}}\alpha_L + C_{M_{L_q}} q_L\right) + V_R^2(\theta_R - \theta_L)\left(C_{M_{R_o}} + C_{M_{R_\alpha}}\alpha_R + C_{M_{R_q}} q_R\right)\right] + \\ \frac{1}{2}\rho V_R^2 S_{t_{ref}}\left[\left(C_{L_{t_{o_R}}} + C_{L_{t_{\alpha_R}}}\alpha_{t_R}\right)\cos(\alpha_{t_R}) + \left(C_{D_{t_{o_R}}} + K\left(C_{L_{t_{o_R}}} + C_{L_{t_{\alpha_R}}}\alpha_{t_R}\right)^2\right)\sin(\alpha_{t_R})\right] x_2 - m_R g x_1\ ] \end{bmatrix} \tag{30}$$

2.5 System Stability Analysis

With the new state vectors in the inertial frame of reference, the full system of equations for both the left and right body of the aircraft were linearized.

$$\vec{x} = [V_L \quad \alpha_L \quad \theta_L \quad q_L \quad V_R \quad \alpha_R \quad \theta_R \quad q_R]^T$$

$$\vec{f} = \dot{\vec{x}} = \left[\dot{V}_L \quad \dot{\alpha}_L \quad \dot{\theta}_L \quad \dot{q}_L \quad \dot{V}_R \quad \dot{\alpha}_R \quad \dot{\theta}_R \quad \dot{q}_R\right]^T \tag{31}$$

With the nominal case, $\Delta x = x(t) - x^o(t)$

$$f(x^0(t) + \Delta x) = f\left(x^o(t)\right) + \left(\frac{\partial f}{\partial x}\right)_o \Delta x + \left(\frac{\partial^2 f}{\partial x^2}\right)_o \Delta x^2 + \left(\frac{\partial^3 f}{\partial x^3}\right)_o \Delta x^3 \ldots$$

Since Δx is small, the higher order terms become negligible as they get closer to zero.

$$\textit{Since, } \dot{x}^o = f^o \tag{32}$$

$$\Delta\dot{x} = \left(\frac{\partial f}{\partial x}\right)_o \Delta x \tag{33}$$

Table 2.1

Partial Derivatives of the State Matrix

$\frac{\partial f_1}{\partial x_1}=\frac{\partial f_1}{\partial V_L}=\phi_{11}$	$\frac{\partial f_1}{\partial x_2}=\frac{\partial f_1}{\partial \alpha_L}=\phi_{12}$	$\frac{\partial f_1}{\partial x_3}=\frac{\partial f_1}{\partial \theta_L}=\phi_{13}$	$\frac{\partial f_1}{\partial x_4}=\frac{\partial f_1}{\partial q_L}=\phi_{14}$	$\frac{\partial f_1}{\partial x_5}=\frac{\partial f_1}{\partial V_R}=0$	$\frac{\partial f_1}{\partial x_6}=\frac{\partial f_1}{\partial \alpha_R}=0$	$\frac{\partial f_1}{\partial x_7}=\frac{\partial f_1}{\partial \theta_R}=0$	$\frac{\partial f_1}{\partial x_8}=\frac{\partial f_1}{\partial q_R}=0$
$\frac{\partial f_2}{\partial x_1}=\frac{\partial f_2}{\partial V_L}=\phi_{21}$	$\frac{\partial f_2}{\partial x_2}=\frac{\partial f_2}{\partial \alpha_L}=\phi_{22}$	$\frac{\partial f_2}{\partial x_3}=\frac{\partial f_2}{\partial \theta_L}=\phi_{23}$	$\frac{\partial f_2}{\partial x_4}=\frac{\partial f_2}{\partial q_L}=\phi_{24}$	$\frac{\partial f_2}{\partial x_5}=\frac{\partial f_2}{\partial V_R}=0$	$\frac{\partial f_2}{\partial x_6}=\frac{\partial f_2}{\partial \alpha_R}=0$	$\frac{\partial f_2}{\partial x_7}=\frac{\partial f_2}{\partial \theta_R}=0$	$\frac{\partial f_2}{\partial x_8}=\frac{\partial f_2}{\partial q_R}=0$
$\frac{\partial f_3}{\partial x_1}=\frac{\partial f_3}{\partial V_L}=0$	$\frac{\partial f_3}{\partial x_2}=\frac{\partial f_3}{\partial \alpha_L}=0$	$\frac{\partial f_3}{\partial x_3}=\frac{\partial f_3}{\partial \theta_L}=0$	$\frac{\partial f_3}{\partial x_4}=\frac{\partial f_3}{\partial q_L}=1$	$\frac{\partial f_3}{\partial x_5}=\frac{\partial f_3}{\partial V_R}=0$	$\frac{\partial f_3}{\partial x_6}=\frac{\partial f_3}{\partial \alpha_R}=0$	$\frac{\partial f_3}{\partial x_7}=\frac{\partial f_3}{\partial \theta_R}=0$	$\frac{\partial f_3}{\partial x_8}=\frac{\partial f_3}{\partial q_R}=0$
$\frac{\partial f_4}{\partial x_1}=\frac{\partial f_4}{\partial V_L}=\phi_{41}$	$\frac{\partial f_4}{\partial x_2}=\frac{\partial f_4}{\partial \alpha_L}=\phi_{42}$	$\frac{\partial f_4}{\partial x_3}=\frac{\partial f_4}{\partial \theta_L}=0$	$\frac{\partial f_4}{\partial x_4}=\frac{\partial f_4}{\partial q_L}=\phi_{44}$	$\frac{\partial f_4}{\partial x_5}=\frac{\partial f_4}{\partial V_R}=\phi_{45}$	$\frac{\partial f_4}{\partial x_6}=\frac{\partial f_4}{\partial \alpha_R}=\phi_{46}$	$\frac{\partial f_4}{\partial x_7}=\frac{\partial f_4}{\partial \theta_R}=\phi_{47}$	$\frac{\partial f_4}{\partial x_8}=\frac{\partial f_4}{\partial q_R}=\phi_{48}$
$\frac{\partial f_5}{\partial x_1}=\frac{\partial f_5}{\partial V_L}=0$	$\frac{\partial f_5}{\partial x_2}=\frac{\partial f_5}{\partial \alpha_L}=0$	$\frac{\partial f_5}{\partial x_3}=\frac{\partial f_5}{\partial \theta_L}=0$	$\frac{\partial f_5}{\partial x_4}=\frac{\partial f_5}{\partial q_L}=0$	$\frac{\partial f_5}{\partial x_5}=\frac{\partial f_5}{\partial V_R}=\phi_{55}$	$\frac{\partial f_5}{\partial x_6}=\frac{\partial f_5}{\partial \alpha_R}=\phi_{56}$	$\frac{\partial f_5}{\partial x_7}=\frac{\partial f_5}{\partial \theta_R}=\phi_{57}$	$\frac{\partial f_5}{\partial x_8}=\frac{\partial f_5}{\partial q_R}=\phi_{58}$
$\frac{\partial f_6}{\partial x_1}=\frac{\partial f_6}{\partial V_L}=0$	$\frac{\partial f_6}{\partial x_2}=\frac{\partial f_6}{\partial \alpha_L}=0$	$\frac{\partial f_6}{\partial x_3}=\frac{\partial f_6}{\partial \theta_L}=0$	$\frac{\partial f_6}{\partial x_4}=\frac{\partial f_6}{\partial q_L}=0$	$\frac{\partial f_6}{\partial x_5}=\frac{\partial f_6}{\partial V_R}=\phi_{65}$	$\frac{\partial f_6}{\partial x_6}=\frac{\partial f_6}{\partial \alpha_R}=\phi_{66}$	$\frac{\partial f_6}{\partial x_7}=\frac{\partial f_6}{\partial \theta_R}=\phi_{67}$	$\frac{\partial f_6}{\partial x_8}=\frac{\partial f_6}{\partial q_R}=\phi_{68}$
$\frac{\partial f_7}{\partial x_1}=\frac{\partial f_7}{\partial V_L}=0$	$\frac{\partial f_7}{\partial x_2}=\frac{\partial f_7}{\partial \alpha_L}=0$	$\frac{\partial f_7}{\partial x_3}=\frac{\partial f_7}{\partial \theta_L}=0$	$\frac{\partial f_7}{\partial x_4}=\frac{\partial f_7}{\partial q_L}=0$	$\frac{\partial f_7}{\partial x_5}=\frac{\partial f_7}{\partial V_R}=0$	$\frac{\partial f_7}{\partial x_6}=\frac{\partial f_7}{\partial \alpha_R}=0$	$\frac{\partial f_7}{\partial x_7}=\frac{\partial f_7}{\partial \theta_R}=0$	$\frac{\partial f_7}{\partial x_8}=\frac{\partial f_7}{\partial q_R}=1$
$\frac{\partial f_8}{\partial x_1}=\frac{\partial f_8}{\partial V_L}=\phi_{81}$	$\frac{\partial f_8}{\partial x_2}=\frac{\partial f_8}{\partial \alpha_L}=\phi_{82}$	$\frac{\partial f_8}{\partial x_3}=\frac{\partial f_8}{\partial \theta_L}=\phi_{83}$	$\frac{\partial f_8}{\partial x_4}=\frac{\partial f_8}{\partial q_L}=\phi_{84}$	$\frac{\partial f_8}{\partial x_5}=\frac{\partial f_8}{\partial V_R}=\phi_{85}$	$\frac{\partial f_8}{\partial x_6}=\frac{\partial f_8}{\partial \alpha_R}=\phi_{86}$	$\frac{\partial f_8}{\partial x_7}=\frac{\partial f_8}{\partial \theta_R}=0$	$\frac{\partial f_8}{\partial x_8}=\frac{\partial f_8}{\partial q_R}=\phi_{88}$

Shown above, the Taylor series expansion of the system about an equilibrium point causes the higher order terms to become negligibly small, so to test the stability of the system, values of the aircraft in different stages of flight that needed to be stable were plugged in to check the system stability.

With the linearized equations of motion, the partial derivatives from the Taylor series expansion generated an 8x8 sensitivity matrix that showed the effects of a certain state variable on another. The coupling effect could be seen here from opposing effects the reactionary moments had on the opposite body of the aircraft.

$$\begin{bmatrix}\dot{V}_L\\ \dot{\alpha}_L\\ \dot{\theta}_L\\ \dot{q}_L\\ \dot{V}_R\\ \dot{\alpha}_R\\ \dot{\theta}_R\\ \dot{q}_R\end{bmatrix}=\begin{bmatrix}\phi_{11} & \phi_{12} & \phi_{13} & \phi_{14} & 0 & 0 & 0 & 0\\ \phi_{21} & \phi_{22} & \phi_{23} & \phi_{24} & 0 & 0 & 0 & 0\\ 0 & 0 & 0 & 1 & 0 & 0 & 0 & 0\\ \phi_{41} & \phi_{42} & 0 & \phi_{44} & \phi_{45} & \phi_{46} & \phi_{47} & \phi_{48}\\ 0 & 0 & 0 & 0 & \phi_{55} & \phi_{56} & \phi_{57} & \phi_{58}\\ 0 & 0 & 0 & 0 & \phi_{65} & \phi_{66} & \phi_{67} & \phi_{68}\\ 0 & 0 & 0 & 0 & 0 & 0 & 0 & 1\\ \phi_{81} & \phi_{82} & \phi_{83} & \phi_{84} & \phi_{85} & \phi_{86} & 0 & \phi_{88}\end{bmatrix}\begin{bmatrix}\Delta V_L\\ \Delta\alpha_L\\ \Delta\theta_L\\ \Delta q_L\\ \dot{V}_R\\ \dot{\alpha}_R\\ \dot{\theta}_R\\ \dot{q}_R\end{bmatrix} \quad (34)$$

$$A = \begin{bmatrix} \phi_{11} & \phi_{12} & \phi_{13} & \phi_{14} & 0 & 0 & 0 & 0 \\ \phi_{21} & \phi_{22} & \phi_{23} & \phi_{24} & 0 & 0 & 0 & 0 \\ 0 & 0 & 0 & 1 & 0 & 0 & 0 & 0 \\ \phi_{41} & \phi_{42} & 0 & \phi_{44} & \phi_{45} & \phi_{46} & \phi_{47} & \phi_{48} \\ 0 & 0 & 0 & 0 & \phi_{55} & \phi_{56} & \phi_{57} & \phi_{58} \\ 0 & 0 & 0 & 0 & \phi_{65} & \phi_{66} & \phi_{67} & \phi_{68} \\ 0 & 0 & 0 & 0 & 0 & 0 & 0 & 1 \\ \phi_{81} & \phi_{82} & \phi_{83} & \phi_{84} & \phi_{85} & \phi_{86} & 0 & \phi_{88} \end{bmatrix} \quad (35)$$

From there, the system needed to be completely observable to continue with the stability analysis. The sensitivity matrix was found to have full rank which meant that the system was observable. All the rows and columns in matrix A were independent which meant that the matrix was fully observable. Next, with the state transition observable, the characteristic equation was determined.

$$Characteristic\ Polynomial = \det(A - I\lambda), \text{ where I is the identity matrix}$$

The full characteristic equation can be found in appendix (I).

This characteristic equation allowed for multiple approaches to analyzing the stability of the system. The roots of the equation would have corresponded to the longitudinal modes of the aircraft in flight. Because the general stability of the unattached tail configuration was desired, a more general approach was taken. To determine the general stability, the Routh-Hurwitz Discriminant was used on the system for an eighth order equation.

$$A\lambda^8 + B\lambda^7 + C\lambda^6 + D\lambda^5 + E\lambda^4 + F\lambda^3 + G\lambda^2 + H\lambda + I \quad (36)$$

Table 2.2

Routh-Hurwitz Array

$$
\begin{array}{c|cccc}
 & A & C & E & G & I \\
 & B & D & F & H & 0 \\
\lambda^8 & \frac{BC-AD}{B} = J & \frac{BE-AF}{B} = K & \frac{BG-AH}{B} = L & I & 0 \\
\lambda^7 & \frac{JD-BK}{J} = M & \frac{JF-BL}{J} = N & \frac{JH-BI}{J} = O & 0 & 0 \\
\lambda^6 & & & & & \\
\lambda^5 & \frac{MK-JN}{M} = P & \frac{ML-JO}{M} = Q & I & 0 & 0 \\
\lambda^4 & & & & & \\
\lambda^3 & \frac{PN-MQ}{P} = R & \frac{(PO-MI)}{P} = S & 0 & 0 & 0 \\
\lambda^2 & & & & & \\
\lambda^1 & \frac{RQ-PS}{R} = T & I & 0 & 0 & 0 \\
\lambda^0 & \frac{(TS-RI)}{T} = U & 0 & 0 & 0 & 0
\end{array}
$$

The Routh-Hurwitz discriminant allowed the system's stability to be analyzed at certain points of flight with a range for certain parameters; however, physical data was needed to use the Routh-Hurwitz analysis method.

Published data about the 747 was used to estimate physical characteristics about the aircraft. Since the Stratolaunch consists of two modified 747 fuselages, the estimations should have yielded close depictions of the aircrafts stability. From the published data, the stability derivatives and physical dimensions were given during different phases of flight including takeoff, cruise, and landing.

Table 2.3

Physical Values Used for Stability Analysis

	Flight Conditions			
Variable	Takeoff Conditions	Climb	Cruise	Cruise
Mass (lbm	560000	620000	620000	620000
Density (lb/ft^3)	0.075	0.075	0.075	0.075
Velocity Left(ft/s)	288	518	830	775
Velocity Right(ft/s)	288	518	830	775
Wing Area (ft^2)	5885	5885	5885	5885
Clol	1.11	0.7	0.266	0.53
Clor	1.12	0.68	0.29	0.521
Clal	5.7	4.67	4.24	4.92
Clar	5.8	4.57	4.2	5.1
alpha l (deg)	5.7	7	0	4.8
alpha r (deg)	5.8	6.8	0	4.6
Cdol	0.102	0.04	0.0174	0.0415
Cdor	0.105	0.0393	0.017	0.04
Thrust Left (lbs)	50000	50000	50000	50000
Thrust Right (lbs)	50500	50500	50500	50500
Cltol	0.5	0.5	0.5	0.5
Cltor	0.6	0.6	0.6	0.6
Cltatl	2.5	2.5	2.5	2.5
Clatr	2.6	2.6	2.6	2.6
u (ft/s)	280	450	830	700
w (ft/s)	67.40919819	256.5619	0	332.6034
ql (deg/s)	0.5	0.4	0	0.6
qr (deg/s)	0.6	0.4	0	0.6
g (ft/s^2)	32.2	32.2	32.2	32.2
Iyy (slug-ft^2)	32300000	33100000	33100000	33100000
alpha tl (deg)	-3	-3	0	-3
alpha tr (deg)	-2.5	-2.5	0	-2.5
Cdtol	0.099	0.099	0.099	0.099
Cdtor	0.095	0.095	0.095	0.095
k	20	20	20	20
cbar (ft)	48	48	48	48
theta left (deg)	3	4	0	2
theta right (deg)	4	5	0	2.5
Cmol	0	0.121	-0.116	0.166
Cmor	0	0.13	-0.12	0.17
Cmql	-20.8	-20.9	-20.5	-24
Cmqr	-21	-20.7	-20.2	-24.2
Cmal	-1.26	-1.25	-0.629	-1.01
Cmar	-1.3	-1.146	-0.7	-1.033
x1 (ft)	20	20	20	20
x2(ft)	150	150	150	150
Ka (lb/ft^2) ?	5.69988E+12	5.7E+12	5.7E+12	5.7E+12
Tail Area (ft^2)	400	400	400	400

The biggest postulation about the aircraft's physical characteristics was the estimation of the composite material's stiffness. Because there is no published information on the actual composite lay-up being used to structure the aircraft, the torsional stiffness of the wing had to be calculated based on estimated values for the composite's properties. To get a conservative value, a very high Young's Modulus (Epsilon) was selected. Multiplying the Young's Modulus value by the cross-sectional moment of inertia generated the estimated stiffness factor of the wing. The cross-sectional moment of inertia was also simplified to be a hollow oval.

$$\text{Wing Stiffness (Ka)} = \text{Young's Modulus } (\epsilon) * \text{Cross sectional moment of inertia (I)}$$

$$Ka = \epsilon I \tag{37}$$

$$I = \frac{\pi}{64}(d_o^4 - d_i^4) \tag{38}$$

d_o & d_i are the outer and inner diameters respectively.

With the wing stiffness values, all the physical properties of the aircraft were estimated, and the Routh-Hurwitz Discriminant generated stability results. The first column calculated from the Routh-Hurwitz Discriminant showed a certain number of sign changes; the number of sign changes corresponded to the number of poles found in the right-hand plane if plotted on a real vs imaginary axis system. Non-negative poles are associated with unstable systems, so if the first column of the RHD generated any sign changes, then the system was unstable at the points used for the aircraft at that point in flight.

Further analysis was done in the cruise conditions of the aircraft. The wing stiffness was focused on by ranging the value of the Young's Modulus for the composite structure wing. This in turn linearly ranged the wing stiffness to analyze the system stability at different stiffness values. Additionally, a ten percent structural damping was added to the wing to supply a damping effect on the system; the structural damping percentage was also ranged to observe the effects. Because the wing was modeled as a torsional spring, the damping factor was needed to force the system to find a stability point. The composite structure of the wing would naturally have a damping effect on the rotation of the two bodies that would add an amount of stability to the system. Moreover, ten percent structural damping was considered to be a conservative amount; anything above a ten percent structural damping value would seem like an unrealistic, and most likely unachievable, amount of structural damping needed for stability.

3. RESULTS

3.1 Aircraft Stability in Take-Off Conditions

The Routh-Hurwitz Discriminant calculated the aircraft's stability at a given equilibrium point with the stiffness of the wing varying based on the Young's Modulus value. With the physical values inputted from the first column in Table 2.3, an equilibrium point that modeled the aircraft in a generic takeoff condition was tested. The aircraft was tested at Mach 0.25 at sea-level with an approximate 5.7-degree angle of attack.

Table 3.1

First Element Column from the Routh Array – Take-Off Conditions

Generic Takeoff Conditions					
Ka = 1	Ka = 2	Ka = 3	Ka = 4	Ka =5	Ka = 6
1	1	1	1	1	1
5484706332.00	109694126.00	1645411900.00	21938336776.00	274231675.10	329082574.10
54694854682.00	309389709.00	464084564.00	6187794187.00	7734742730.00	928191280.00
429216437.00	858432874.00	1287649311.00	17168657486.00	21460821.00	2575298.00
3271580956.00	6546831619.00	9820247428.00	1309366.32	1636707.00	19473953.00
54349612322.00	86992246.00	163048836.00	7398449289.16	27174861.14	32609769.34
54404623932.00	88092478658.00	16321179880.00	217618.50	2720231.20	2642774.36
-2589635797.00	-5179271595.00	7768907393.00	1035859093.00	1789886882.00	531444500.00

The results showed that the system was unstable for the given physical values and selected trim point. In the table, each column corresponds to the first-column elements in the Routh array for a given wing stiffness. Wing stiffness was varied from an underestimated value to an overestimated value. For the system to be stable, the first-column elements in the Routh array should not have any sign changes. Each sign change corresponds to the system having a positive eigenvector root, or a pole in the right-hand plane of the real vs imaginary axis system which indicates instability in the system. For

the lowest two spring constant values corresponding to Ka = 1 and Ka = 2, there appeared one sign change in the first column elements of the Routh array. This sign change indicated there one eigenvalue would be a positive value showing indicating an unstable mode. The rest of the spring stiffness values had no sign changes in the Routh array, thus it could be deduced that the system was at least stable for those values.

3.2 Aircraft Stability in Climb Conditions

Next, physical values found in the second column of Table 3 were inputted to reflect a general climb condition of the aircraft. The same exercise was repeated to check for stability of the system at the new equilibrium point; the aircraft was modelled at Mach 0.5 at 20,000 feet with an approximate 6.8-degree angle of attack.

Table 3.2

First Element Column from the Routh Array – Climb Conditions

Generic Climb Conditions					
Ka = 1	Ka = 2	Ka = 3	Ka = 4	Ka =5	Ka = 6
1.00	1.00	1.00	1.00	1.00	1.00
1739745.10	34794889.40	5219232668.00	695897689.00	869872111.00	10438465.00
45479755.00	9095951.00	136439265.00	1819190201.00	227398775.00	272878530.00
40225405.00	45081024.00	2067621537.00	1609016204.00	20112702.00	2135243.00
133431191.00	2668623839.00	400293575.00	5337247679.00	6155959958.00	80058715.00
1349661413.00	2699322826.00	404898423.00	5398645653.00	67483070.00	9796847980.00
-233913463.00	-4678269.00	174039087.00	93565385450.00	116956731.00	1403480781.00

From the Routh-Hurwitz discriminant, similar results were found. Each column in Table 3.2 corresponds to the first-column elements in the Routh array for the aircraft with a given wing stiffness. For one of the modes in the climb stage, the first-column elements of the Routh array again had one positive, non-zero root in the right-hand plane for the two lowest spring constants. The analysis showed that in this climb configuration the system was unstable about the given equilibrium point for those spring constant values.

As the torsional stiffness of the spring increased, the first column elements of the Routh array had no sign changes showing the system was stable.

3.3 Aircraft Stability in Cruise Conditions

Continuing with the analysis, two cruise conditions were tested with the same approach. From the third column of Table 4, physical data was inputted to reflect a zero angle of attack cruise condition at Mach 0.8 at 20,000 feet.

Table 3.3

First Element Column from the Routh Array – Cruise Conditions

Generic Cruise Conditions					
Ka = 1	Ka = 2	Ka = 3	Ka = 4	Ka =5	Ka = 6
1.00	1.00	1.00	1.00	1.00	1.00
223596.00	44719222.00	67077464.50	8943889.10	1117980.00	1341576674.00
2103835.00	42076637.00	631149561.00	841532748.00	105191593.00	12622953.00
570180512.00	114036102.00	1710541536.00	22807220.00	2850902560.00	342108307.00
827568269.00	16551365.00	248270480.00	3310273077.00	41378413.00	496540961.00
508471251.00	101694250.00	15254137.00	203388500.00	25423562.00	305082.00
5091364.00	101827283.00	1527409259.00	2036545679.00	254568209.00	30548185.00
-223028999.00	-44605799.00	66908699968.00	89219958.00	11151449.00	133817399.00

Each column again represents the first-column elements of the Routh array at a specific wing thickness. The trend continued for climb where the two lowest spring constant values had one sign change – the eigenvalues of the system would have at least one non-zero, positive value. Moreover, the sign changes in the first-column elements signified that the aircraft was unstable at the given equilibrium point applied. Similarly, as the spring constant increased, no sign changes occurred which indicated the system was stable for those values.

3.4 Aircraft Stability in Post-Separation Conditions

The final condition test was a high altitude, high speed, and positive angle of attack flight scenario; this condition could potentially apply to the aircraft's flight plan after the drop of the payload mid-flight. The physical data was inputted for Mach 0.8 at 40,000 feet with an approximate 4.6-degree angle of attack.

Table 3.4

First Element Column from the Routh Array – Cruise/Payload Drop Conditions

Generic Post-Separation Conditions					
Ka = 1	Ka = 2	Ka = 3	Ka = 4	Ka =5	Ka = 6
1.00	1.00	1.00	1.00	1.00	1.00
22359592.40	44711216.90	670841.50	894386.00	1117980.00	1341576.00
71832148.00	1436290.00	215430640.00	28724081.00	35905101.00	4308612.00
7159513454.00	1431902.00	21478540.00	286380.00	35797567.00	42957080.00
360554770.00	72110954.00	1081660.00	1442219.00	1802773.00	21633286.00
74337997.00	148675995.00	22301399.00	29735199.00	37168998.00	446027986.00
1042896.00	20857928.00	31286892.00	4171585.00	5214482.00	625737852.00
-79564851.71	-15812664.50	2371877.40	316244.00	3959103.10	4743670.00

The general trend also continued with the final case; each column contains the first-column elements of the Routh array at a given wing stiffness value. The two lowest spring constant values had one sign change in the first-column element array which showed that the system has one non-zero, positive eigenvalue in the right-hand plane. The non-zero, positive roots signify that the system is unstable at the given equilibrium point for those spring constant values. Again, as the spring constant increased the first-column elements had no sign changes indicating system stability.

The general results gathered from the four common flight conditions entered for the system all signified that the system would be unstable with a low enough spring constant value even with a conservative structural damping effect.

3.5 System Eigenvalues

To get a better understanding of the modes occurring for the ranging stiffness values, the eigenvalues corresponding to each value of wing stiffness was plotted on the real and imaginary axes for the cruise condition case. The highlighted circles that appear on the eigenvalues indicate the high value for the spring constant; as the eigenvalues move with the decreasing constant value, the last point with the lowest constant value is indicated with a highlighted "x" character. The initial spring constant value was calculated from Eq. (37) using the conservative Young's Modulus value for a carbon composite material.

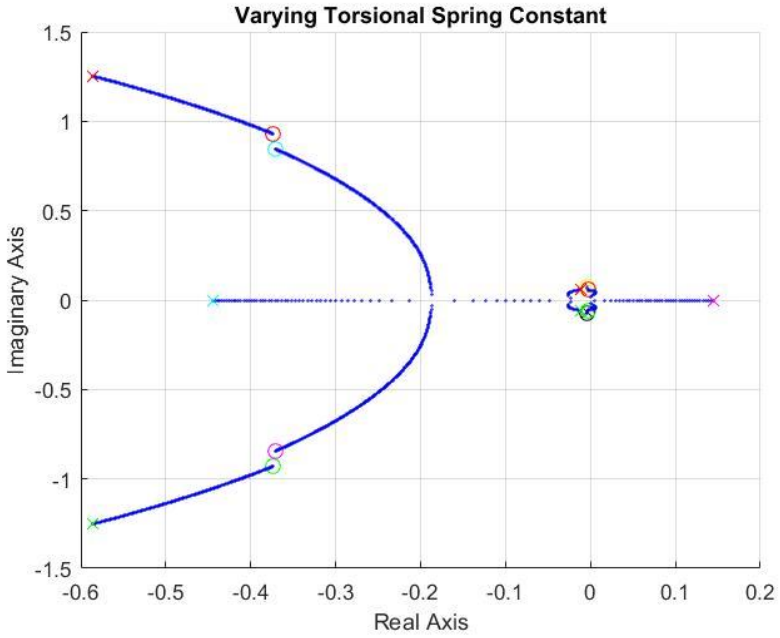

Fig. 3.1 Eigenvalues when ranging torsional spring constant in cruise.

Expectantly, the system had eigenvalues in the right-hand plane of figure 3.1 as the torsional spring constant continued to decrease. The torsional spring constant influenced both the frequencies of the two bodies' short-period modes and the overshoot envelope for the short period modes of both bodies. As the spring constant decreased, the change in frequency between the modes of the two bodies continued to get larger and larger. One of the body's short period frequency increased while the other's decreased until it finally collapsed on to the real axis. Furthermore, the phugoid modes of both bodies remained steady until one of the modes also collapsed on to the real axis with one eigenvalue becoming real and positive.

Additionally, for the most conservative spring stiffness value, the structural damping was ranged from ten percent to two percent in the cruise condition. The structural damping was also expected to help keep the system stable at the high, conservative percentage, and the effects of lowering the structural damping were recorded using the same method as for the torsional spring constant.

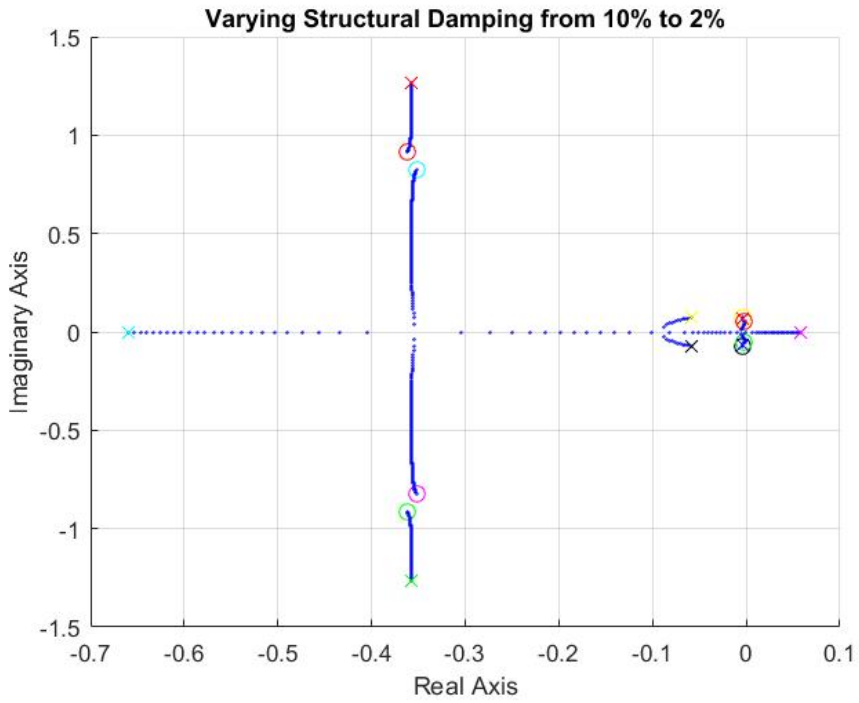

Fig. 3.2 Eigenvalues when varying structural damping in cruise.

The structural damping also had a threshold percentage where the system would become unstable if the damping value was too low. Similarly, to the effects of the spring constant, when the structural damping dipped below 4 percent one of each of the short period and phugoid modes collapsed on to the real axis, with one of the phugoid modes becoming unstable.

The unstable cases from both the insufficient spring torsion value and low structural damping indicates that the system is always a non-minimum phase system. These systems can have significantly slow responses to system inputs and can in general be difficult to implement active control systems effectively.

Finally, to validate the results and eigenvalues gathered, the system was tested with the two bodies of the aircraft uncoupled, virtually a non-existent spring constant and no structural damping present, and the eigenvalues were recorded.

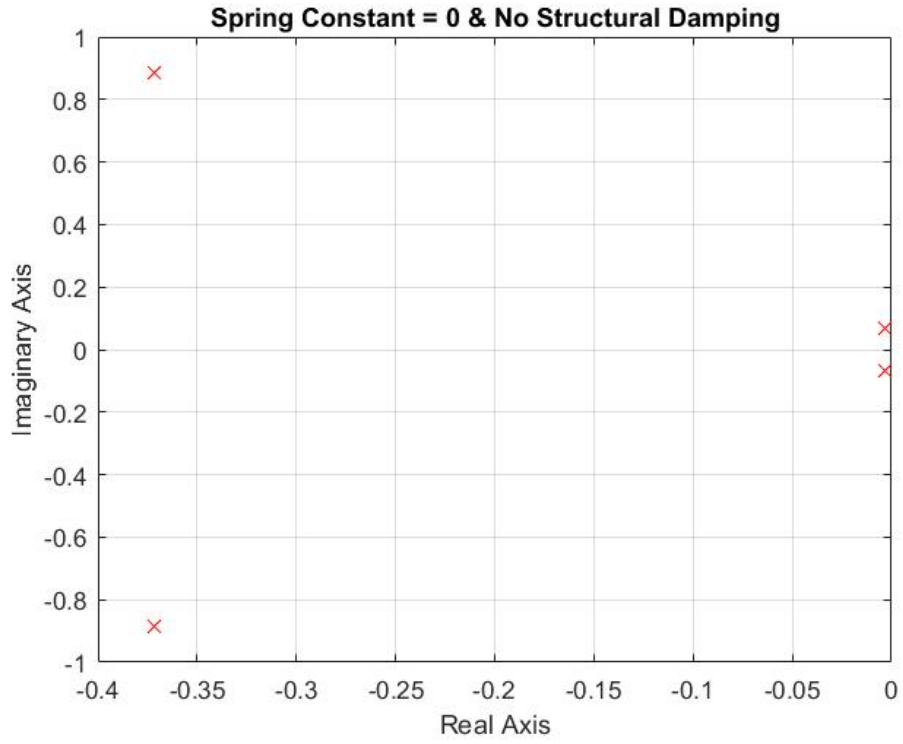

Fig. 3.3 Eigenvalues of the uncoupled aircraft without structural damping in cruise.

The results verified that the model accurately represented two single body 747 aircraft because the two sets of modes, the short period and phugoid, matched published data of the longitudinal modes of a tested 747 in cruise. The plot appears to only have four eigenvalues; however, the second set of modes overlay the first exactly due to the uncoupled moment effects which is why the model behaves as two independent aircraft.

Additionally, with a high, conservative structural damping, the spring constant was set to approach infinity for the aircraft in the cruise conditions, and the eigenvalues were recorded.

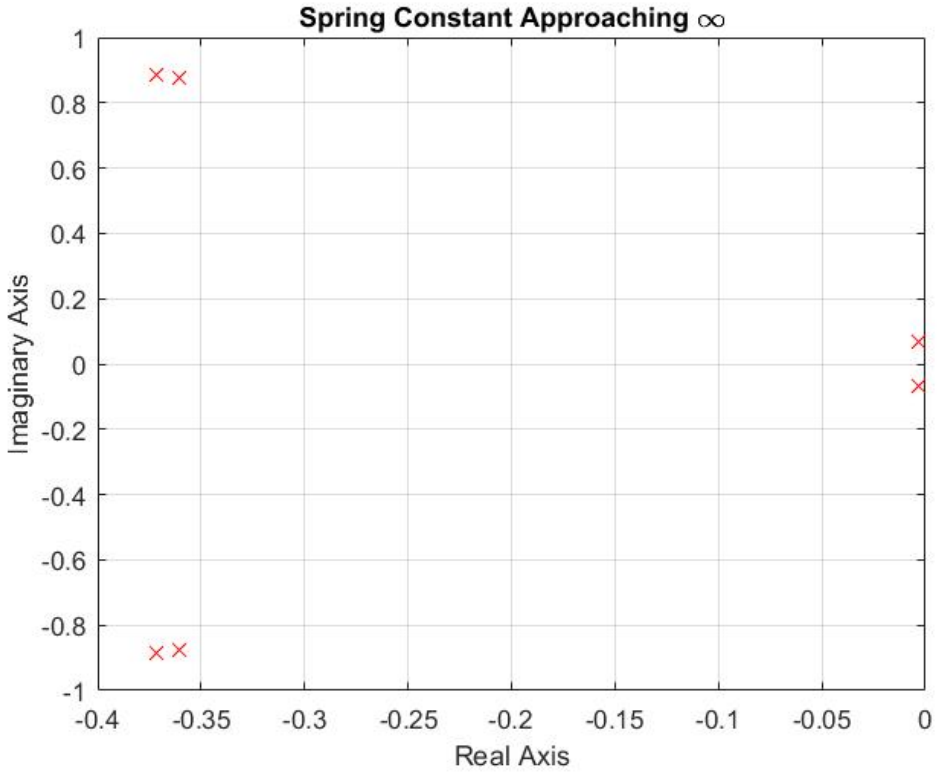

Fig. 3.4 Eigenvalues of the aircraft as the spring constant approaches infinity.

The system begins to converge towards the published data of the 747 with the phugoid modes overlaying for the two bodies and the frequencies between the short period modes of the two bodies becoming virtually the same.

4. CONCLUSIONS

This thesis takes a closer look at one of the pioneering methods of reducing cost to reach space for commercial and private purposes. Two very similar carrier aircraft,

acting as reusable air-breathing first stages, have been proposed. This thesis presented the development and results from a stability analysis of one of them, the Vulcan Aerospace's Stratolaunch carrier aircraft, to determine its feasibility. The proposed design, currently under construction for first flight, will have the largest wingspan of any aircraft ever built. The question posed in this thesis is whether the unattached twin tail design will be stable for an aircraft of that size. The aircraft was modeled with the wing acting as a torsional spring with the twin fuselages attached. Since the fuselages of the aircraft are modified Boeing 747 fuselages, published data for the 747 was used to generate stability derivatives. Four flight conditions were analyzed: take-off, climb, cruise, and aircraft orientation immediately after the payload drop. All four cases were analyzed using Routh-Hurwitz stability criterion, and the discriminant for all four cases showed that the aircraft was unstable in the longitudinal plane when either the torsional spring constant or structural damping value became too small. In the cruise condition, the phugoid mode would collapse first on to the real axis with a positive value zero in the right-hand plane – which revealed the system to be an unstable, non-minimum phase system. With the spring constant decreasing further the short period mode would also become unstable resulting in total system instability. The results suggest the success of a twin fuselage aircraft with unattached tails would rely on the composite material being used and its natural damping effects, and the torsional stiffness of the wing. With the latter being a potential design point of the aircraft, a similar aircraft design could improve stability in the design phase; however, the structural damping effect relies on technological advancements of composite materials.

Looking forward, for the viability of large air-breathing, reusable first stages for space launch vehicles, potential solutions should be explored to ensure the stability of these aircraft. Moreover, if the demand for larger payloads is going to continue to drive the size of these aircraft up, then alternative designs or alterations will be needed. The structural damping used in this thesis was a very conservative value that most likely could not be duplicated in practice due to cost effectiveness. A potential solution could be to connect the two tails of the aircraft. The aircraft design could be modified to reach the same flight results and adding an extra structural component should increase structural rigidity and decrease the oscillating mode. A composite connection between the tails would also be a light enough mass addition that shouldn't hurt the payload capability as well.

The possibilities for achieving cheap and reliable access to space for both the commercial and private industry are endless, and the question is not if that goal will be achieved, but when. The air-breathing reusable first stage has already proved its viability in the space launch industry, and whereas an aircraft as large as the Stratolaunch may pose difficulties in practice, the adjustments will continue to be made to one day make spaceflight as common as booking an airline ticket.

5. REFERENCES

Etkin, Bernard, and Lloyd Duff. Reid. *Dynamics of flight: stability and control*. New York: J. Wiley & Sons, 1996. Print.

Grantham, William D., Perry L. Deal, Gerald L. Keyser, Jr., and Paul M. Smith. "Simulator Study of Flight Characteristics of a Large Twin-Fuselage Cargo Transport Airplane during Approach and Landing." *NASA Technical Paper* 2183 (1983): n. pag. Web.

Kabamba, Pierre T., and Anouck R. Girard. *Fundamentals of aerospace navigation and guidance*. New York: Cambridge U Press, 2014. Print.

Napolitano, Marcello R. *Aircraft dynamics: from modeling to simulation*. Hoboken, NJ: Wiley, 2012. Print.

Weingarten, N. C., and C. R. Chalk. "In-flight investigation of large airplane flying qualities for approach and landing." *Journal of Guidance, Control, and Dynamics* 7.1 (1984): 92-98. Web.

“Stratolaunch.” *Stratolaunch.* Vulcan Aerospace, n.d. Web. 15 Sept. 2016.

APPENDIX I

FULLLY DERIVED CHARACTERISTIC EQUATION

Full Form Characteristic Equation (where the $a_{i^{th}j^{th}}$ coefficients correspond to the partial derivate of that element in the sensitivity matrix):

lambda^8 + (- a11 - a22 - a44 - a55 - a66 - a88)*lambda^7 + (a11*a22 - a12*a21 + a11*a44 - a14*a41 + a11*a55 + a22*a44 - a24*a42 + a11*a66 + a22*a55 + a22*a66 + a11*a88 + a44*a55 + a22*a88 + a44*a66 + a55*a66 - a56*a65 + a44*a88 - a48*a84 + a55*a88 - a58*a85 + a66*a88 - a68*a86)*lambda^6 + (a11*a24*a42 - a23*a42 - a47*a84 - a48*a83 - a57*a85 - a67*a86 - a11*a22*a44 - a13*a41 + a12*a21*a44 - a12*a24*a41 - a14*a21*a42 + a14*a22*a41 - a11*a22*a55 + a12*a21*a55 - a11*a22*a66 + a12*a21*a66 - a11*a44*a55 + a14*a41*a55 - a11*a22*a88 - a11*a44*a66 + a12*a21*a88 + a14*a41*a66 - a22*a44*a55 + a24*a42*a55 - a11*a55*a66 + a11*a56*a65 - a22*a44*a66 + a24*a42*a66 - a11*a44*a88 + a11*a48*a84 + a14*a41*a88 - a14*a48*a81 - a22*a55*a66 + a22*a56*a65 - a11*a55*a88 + a11*a58*a85 - a22*a44*a88 + a22*a48*a84 + a24*a42*a88 - a24*a48*a82 - a11*a66*a88 + a11*a68*a86 - a22*a55*a88 + a22*a58*a85 - a44*a55*a66 + a44*a56*a65 - a22*a66*a88 + a22*a68*a86 - a44*a55*a88 + a44*a58*a85 - a45*a58*a84 + a48*a55*a84 - a44*a66*a88 + a44*a68*a86 - a46*a68*a84 + a48*a66*a84 - a55*a66*a88 + a55*a68*a86 + a56*a65*a88 - a56*a68*a85 - a58*a65*a86 + a58*a66*a85)*lambda^5 + (a11*a23*a42 - a47*a83 - a12*a23*a41 - a13*a21*a42 + a13*a22*a41 + a13*a41*a55 + a13*a41*a66 + a23*a42*a55 + a23*a42*a66 + a11*a47*a84 + a11*a48*a83 + a13*a41*a88 - a13*a48*a81 - a14*a47*a81 + a11*a57*a85 + a22*a47*a84 + a22*a48*a83 + a23*a42*a88 - a23*a48*a82 - a24*a47*a82 + a11*a67*a86 + a22*a57*a85 + a22*a67*a86 + a44*a57*a85 - a45*a57*a84 - a45*a58*a83 + a47*a55*a84 + a48*a55*a83 + a44*a67*a86 - a46*a67*a84 - a46*a68*a83 + a47*a66*a84 + a48*a66*a83 + a55*a67*a86 - a56*a67*a85 - a57*a65*a86 + a57*a66*a85 + a11*a22*a44*a55 - a11*a24*a42*a55 - a12*a21*a44*a55 + a12*a24*a41*a55 + a14*a21*a42*a55 - a14*a22*a41*a55 + a11*a22*a44*a66 - a11*a24*a42*a66 - a12*a21*a44*a66 + a12*a24*a41*a66 + a14*a21*a42*a66 - a14*a22*a41*a66 + a11*a22*a55*a66 - a11*a22*a56*a65 - a12*a21*a55*a66 + a12*a21*a56*a65 + a11*a22*a44*a88 - a11*a22*a48*a84 - a11*a24*a42*a88 + a11*a24*a48*a82 - a12*a21*a44*a88 + a12*a21*a48*a84 + a12*a24*a41*a88 - a12*a24*a48*a81 + a14*a21*a42*a88 - a14*a21*a48*a82 - a14*a22*a41*a88 + a14*a22*a48*a81 + a11*a22*a55*a88 - a11*a22*a58*a85 + a11*a44*a55*a66 - a11*a44*a56*a65 - a12*a21*a55*a88 + a12*a21*a58*a85 - a14*a41*a55*a66 + a14*a41*a56*a65 + a11*a22*a66*a88 - a11*a22*a68*a86 - a12*a21*a66*a88 + a12*a21*a68*a86 + a22*a44*a55*a66 - a22*a44*a56*a65 - a24*a42*a55*a66 + a24*a42*a56*a65 + a11*a44*a55*a88 - a11*a44*a58*a85 + a11*a45*a58*a84 - a11*a48*a55*a84 - a14*a41*a55*a88 + a14*a41*a58*a85 - a14*a45*a58*a81 + a14*a48*a55*a81 + a11*a44*a66*a88 - a11*a44*a68*a86 + a11*a46*a68*a84 - a11*a48*a66*a84 - a14*a41*a66*a88 + a14*a41*a68*a86 - a14*a46*a68*a81 + a14*a48*a66*a81 + a22*a44*a55*a88 - a22*a44*a58*a85 + a22*a45*a58*a84 - a22*a48*a55*a84 - a24*a42*a55*a88 + a24*a42*a58*a85 - a24*a45*a58*a82 + a24*a48*a55*a82 +

a11*a55*a66*a88 - a11*a55*a68*a86 - a11*a56*a65*a88 + a11*a56*a68*a85 + a11*a58*a65*a86 - a11*a58*a66*a85 + a22*a44*a66*a88 - a22*a44*a68*a86 + a22*a46*a68*a84 - a22*a48*a66*a84 - a24*a42*a66*a88 + a24*a42*a68*a86 - a24*a46*a68*a82 + a24*a48*a66*a82 + a22*a55*a66*a88 - a22*a55*a68*a86 - a22*a56*a65*a88 + a22*a56*a68*a85 + a22*a58*a65*a86 - a22*a58*a66*a85 + a44*a55*a66*a88 - a44*a55*a68*a86 - a44*a56*a65*a88 + a44*a56*a68*a85 + a44*a58*a65*a86 - a44*a58*a66*a85 - a45*a56*a68*a84 + a45*a58*a66*a84 + a46*a55*a68*a84 - a46*a58*a65*a84 - a48*a55*a66*a84 + a48*a56*a65*a84)*lambda^4 + (a11*a47*a83 - a13*a47*a81 + a22*a47*a83 - a23*a47*a82 - a45*a57*a83 + a47*a55*a83 - a46*a67*a83 + a47*a66*a83 - a11*a23*a42*a55 + a12*a23*a41*a55 + a13*a21*a42*a55 - a13*a22*a41*a55 - a11*a23*a42*a66 + a12*a23*a41*a66 + a13*a21*a42*a66 - a13*a22*a41*a66 - a11*a22*a47*a84 - a11*a22*a48*a83 - a11*a23*a42*a88 + a11*a23*a48*a82 + a11*a24*a47*a82 + a12*a21*a47*a84 + a12*a21*a48*a83 + a12*a23*a41*a88 - a12*a23*a48*a81 - a12*a24*a47*a81 + a13*a21*a42*a88 - a13*a21*a48*a82 - a13*a22*a41*a88 + a13*a22*a48*a81 - a14*a21*a47*a82 + a14*a22*a47*a81 - a11*a22*a57*a85 + a12*a21*a57*a85 - a13*a41*a55*a66 + a13*a41*a56*a65 - a11*a22*a67*a86 + a12*a21*a67*a86 - a23*a42*a55*a66 + a23*a42*a56*a65 - a11*a44*a57*a85 + a11*a45*a57*a84 + a11*a45*a58*a83 - a11*a47*a55*a84 - a11*a48*a55*a83 - a13*a41*a55*a88 + a13*a41*a58*a85 - a13*a45*a58*a81 + a13*a48*a55*a81 + a14*a41*a57*a85 - a14*a45*a57*a81 + a14*a47*a55*a81 - a11*a44*a67*a86 + a11*a46*a67*a84 + a11*a46*a68*a83 - a11*a47*a66*a84 - a11*a48*a66*a83 - a13*a41*a66*a88 + a13*a41*a68*a86 - a13*a46*a68*a81 + a13*a48*a66*a81 + a14*a41*a67*a86 - a14*a46*a67*a81 + a14*a47*a66*a81 - a22*a44*a57*a85 + a22*a45*a57*a84 + a22*a45*a58*a83 - a22*a47*a55*a84 - a22*a48*a55*a83 - a23*a42*a55*a88 + a23*a42*a58*a85 - a23*a45*a58*a82 + a23*a48*a55*a82 + a24*a42*a57*a85 - a24*a45*a57*a82 + a24*a47*a55*a82 - a11*a55*a67*a86 + a11*a56*a67*a85 + a11*a57*a65*a86 - a11*a57*a66*a85 - a22*a44*a67*a86 + a22*a46*a67*a84 + a22*a46*a68*a83 - a22*a47*a66*a84 - a22*a48*a66*a83 - a23*a42*a66*a88 + a23*a42*a68*a86 - a23*a46*a68*a82 + a23*a48*a66*a82 + a24*a42*a67*a86 - a24*a46*a67*a82 + a24*a47*a66*a82 - a22*a55*a67*a86 + a22*a56*a67*a85 + a22*a57*a65*a86 - a22*a57*a66*a85 - a44*a55*a67*a86 + a44*a56*a67*a85 + a44*a57*a65*a86 - a44*a57*a66*a85 - a45*a56*a67*a84 - a45*a56*a68*a83 + a45*a57*a66*a84 + a45*a58*a66*a83 + a46*a55*a67*a84 + a46*a55*a68*a83 - a46*a57*a65*a84 - a46*a58*a65*a83 - a47*a55*a66*a84 + a47*a56*a65*a84 - a48*a55*a66*a83 + a48*a56*a65*a83 - a11*a22*a44*a55*a66 + a11*a22*a44*a56*a65 + a11*a24*a42*a55*a66 - a11*a24*a42*a56*a65 + a12*a21*a44*a55*a66 - a12*a21*a44*a56*a65 - a12*a24*a41*a55*a66 + a12*a24*a41*a56*a65 - a14*a21*a42*a55*a66 + a14*a21*a42*a56*a65 + a14*a22*a41*a55*a66 - a14*a22*a41*a56*a65 - a11*a22*a44*a55*a88 + a11*a22*a44*a58*a85 - a11*a22*a45*a58*a84 + a11*a22*a48*a55*a84 + a11*a24*a42*a55*a88 - a11*a24*a42*a58*a85 +

a11*a24*a45*a58*a82 - a11*a24*a48*a55*a82 + a12*a21*a44*a55*a88 - a12*a21*a44*a58*a85 + a12*a21*a45*a58*a84 - a12*a21*a48*a55*a84 - a12*a24*a41*a55*a88 + a12*a24*a41*a58*a85 - a12*a24*a45*a58*a81 + a12*a24*a48*a55*a81 - a14*a21*a42*a55*a88 + a14*a21*a42*a58*a85 - a14*a21*a45*a58*a82 + a14*a21*a48*a55*a82 + a14*a22*a41*a55*a88 - a14*a22*a41*a58*a85 + a14*a22*a45*a58*a81 - a14*a22*a48*a55*a81 - a11*a22*a44*a66*a88 + a11*a22*a44*a68*a86 - a11*a22*a46*a68*a84 + a11*a22*a48*a66*a84 + a11*a24*a42*a66*a88 - a11*a24*a42*a68*a86 + a11*a24*a46*a68*a82 - a11*a24*a48*a66*a82 + a12*a21*a44*a66*a88 - a12*a21*a44*a68*a86 + a12*a21*a46*a68*a84 - a12*a21*a48*a66*a84 - a12*a24*a41*a66*a88 + a12*a24*a41*a68*a86 - a12*a24*a46*a68*a81 + a12*a24*a48*a66*a81 - a14*a21*a42*a66*a88 + a14*a21*a42*a68*a86 - a14*a21*a46*a68*a82 + a14*a21*a48*a66*a82 + a14*a22*a41*a66*a88 - a14*a22*a41*a68*a86 + a14*a22*a46*a68*a81 - a14*a22*a48*a66*a81 - a11*a22*a55*a66*a88 + a11*a22*a55*a68*a86 + a11*a22*a56*a65*a88 - a11*a22*a56*a68*a85 - a11*a22*a58*a65*a86 + a11*a22*a58*a66*a85 + a12*a21*a55*a66*a88 - a12*a21*a55*a68*a86 - a12*a21*a56*a65*a88 + a12*a21*a56*a68*a85 + a12*a21*a58*a65*a86 - a12*a21*a58*a66*a85 - a11*a44*a55*a66*a88 + a11*a44*a55*a68*a86 + a11*a44*a56*a65*a88 - a11*a44*a56*a68*a85 - a11*a44*a58*a65*a86 + a11*a44*a58*a66*a85 + a11*a45*a56*a68*a84 - a11*a45*a58*a66*a84 - a11*a46*a55*a68*a84 + a11*a46*a58*a65*a84 + a11*a48*a55*a66*a84 - a11*a48*a56*a65*a84 + a14*a41*a55*a66*a88 - a14*a41*a55*a68*a86 - a14*a41*a56*a65*a88 + a14*a41*a56*a68*a85 + a14*a41*a58*a65*a86 - a14*a41*a58*a66*a85 - a14*a45*a56*a68*a81 + a14*a45*a58*a66*a81 + a14*a46*a55*a68*a81 - a14*a46*a58*a65*a81 - a14*a48*a55*a66*a81 + a14*a48*a56*a65*a81 - a22*a44*a55*a66*a88 + a22*a44*a55*a68*a86 + a22*a44*a56*a65*a88 - a22*a44*a56*a68*a85 - a22*a44*a58*a65*a86 + a22*a44*a58*a66*a85 + a22*a45*a56*a68*a84 - a22*a45*a58*a66*a84 - a22*a46*a55*a68*a84 + a22*a46*a58*a65*a84 + a22*a48*a55*a66*a84 - a22*a48*a56*a65*a84 + a24*a42*a55*a66*a88 - a24*a42*a55*a68*a86 - a24*a42*a56*a65*a88 + a24*a42*a56*a68*a85 + a24*a42*a58*a65*a86 - a24*a42*a58*a66*a85 - a24*a45*a56*a68*a82 + a24*a45*a58*a66*a82 + a24*a46*a55*a68*a82 - a24*a46*a58*a65*a82 - a24*a48*a55*a66*a82 + a24*a48*a56*a65*a82)*lambda^3 + (a11*a23*a47*a82 - a11*a22*a47*a83 + a12*a21*a47*a83 - a12*a23*a47*a81 - a13*a21*a47*a82 + a13*a22*a47*a81 + a11*a45*a57*a83 - a11*a47*a55*a83 + a13*a41*a57*a85 - a13*a45*a57*a81 + a13*a47*a55*a81 + a11*a46*a67*a83 - a11*a47*a66*a83 + a13*a41*a67*a86 - a13*a46*a67*a81 + a13*a47*a66*a81 + a22*a45*a57*a83 - a22*a47*a55*a83 + a23*a42*a57*a85 - a23*a45*a57*a82 + a23*a47*a55*a82 + a22*a46*a67*a83 - a22*a47*a66*a83 + a23*a42*a67*a86 - a23*a46*a67*a82 + a23*a47*a66*a82 - a45*a56*a67*a83 + a45*a57*a66*a83 + a46*a55*a67*a83 - a46*a57*a65*a83 - a47*a55*a66*a83 + a47*a56*a65*a83 +

a11*a23*a42*a55*a66 - a11*a23*a42*a56*a65 - a12*a23*a41*a55*a66 +
a12*a23*a41*a56*a65 - a13*a21*a42*a55*a66 + a13*a21*a42*a56*a65 +
a13*a22*a41*a55*a66 - a13*a22*a41*a56*a65 + a11*a22*a44*a57*a85 -
a11*a22*a45*a57*a84 - a11*a22*a45*a58*a83 + a11*a22*a47*a55*a84 +
a11*a22*a48*a55*a83 + a11*a23*a42*a55*a88 - a11*a23*a42*a58*a85 +
a11*a23*a45*a58*a82 - a11*a23*a48*a55*a82 - a11*a24*a42*a57*a85 +
a11*a24*a45*a57*a82 - a11*a24*a47*a55*a82 - a12*a21*a44*a57*a85 +
a12*a21*a45*a57*a84 + a12*a21*a45*a58*a83 - a12*a21*a47*a55*a84 -
a12*a21*a48*a55*a83 - a12*a23*a41*a55*a88 + a12*a23*a41*a58*a85 -
a12*a23*a45*a58*a81 + a12*a23*a48*a55*a81 + a12*a24*a41*a57*a85 -
a12*a24*a45*a57*a81 + a12*a24*a47*a55*a81 - a13*a21*a42*a55*a88 +
a13*a21*a42*a58*a85 - a13*a21*a45*a58*a82 + a13*a21*a48*a55*a82 +
a13*a22*a41*a55*a88 - a13*a22*a41*a58*a85 + a13*a22*a45*a58*a81 -
a13*a22*a48*a55*a81 + a14*a21*a42*a57*a85 - a14*a21*a45*a57*a82 +
a14*a21*a47*a55*a82 - a14*a22*a41*a57*a85 + a14*a22*a45*a57*a81 -
a14*a22*a47*a55*a81 + a11*a22*a44*a67*a86 - a11*a22*a46*a67*a84 -
a11*a22*a46*a68*a83 + a11*a22*a47*a66*a84 + a11*a22*a48*a66*a83 +
a11*a23*a42*a66*a88 - a11*a23*a42*a68*a86 + a11*a23*a46*a68*a82 -
a11*a23*a48*a66*a82 - a11*a24*a42*a67*a86 + a11*a24*a46*a67*a82 -
a11*a24*a47*a66*a82 - a12*a21*a44*a67*a86 + a12*a21*a46*a67*a84 +
a12*a21*a46*a68*a83 - a12*a21*a47*a66*a84 - a12*a21*a48*a66*a83 -
a12*a23*a41*a66*a88 + a12*a23*a41*a68*a86 - a12*a23*a46*a68*a81 +
a12*a23*a48*a66*a81 + a12*a24*a41*a67*a86 - a12*a24*a46*a67*a81 +
a12*a24*a47*a66*a81 - a13*a21*a42*a66*a88 + a13*a21*a42*a68*a86 -
a13*a21*a46*a68*a82 + a13*a21*a48*a66*a82 + a13*a22*a41*a66*a88 -
a13*a22*a41*a68*a86 + a13*a22*a46*a68*a81 - a13*a22*a48*a66*a81 +
a14*a21*a42*a67*a86 - a14*a21*a46*a67*a82 + a14*a21*a47*a66*a82 -
a14*a22*a41*a67*a86 + a14*a22*a46*a67*a81 - a14*a22*a47*a66*a81 +
a11*a22*a55*a67*a86 - a11*a22*a56*a67*a85 - a11*a22*a57*a65*a86 +
a11*a22*a57*a66*a85 - a12*a21*a55*a67*a86 + a12*a21*a56*a67*a85 +
a12*a21*a57*a65*a86 - a12*a21*a57*a66*a85 + a11*a44*a55*a67*a86 -
a11*a44*a56*a67*a85 - a11*a44*a57*a65*a86 + a11*a44*a57*a66*a85 +
a11*a45*a56*a67*a84 + a11*a45*a56*a68*a83 - a11*a45*a57*a66*a84 -
a11*a45*a58*a66*a83 - a11*a46*a55*a67*a84 - a11*a46*a55*a68*a83 +
a11*a46*a57*a65*a84 + a11*a46*a58*a65*a83 + a11*a47*a55*a66*a84 -
a11*a47*a56*a65*a84 + a11*a48*a55*a66*a83 - a11*a48*a56*a65*a83 +
a13*a41*a55*a66*a88 - a13*a41*a55*a68*a86 - a13*a41*a56*a65*a88 +
a13*a41*a56*a68*a85 + a13*a41*a58*a65*a86 - a13*a41*a58*a66*a85 -
a13*a45*a56*a68*a81 + a13*a45*a58*a66*a81 + a13*a46*a55*a68*a81 -
a13*a46*a58*a65*a81 - a13*a48*a55*a66*a81 + a13*a48*a56*a65*a81 -
a14*a41*a55*a67*a86 + a14*a41*a56*a67*a85 + a14*a41*a57*a65*a86 -
a14*a41*a57*a66*a85 - a14*a45*a56*a67*a81 + a14*a45*a57*a66*a81 +

a14*a46*a55*a67*a81 - a14*a46*a57*a65*a81 - a14*a47*a55*a66*a81 + a14*a47*a56*a65*a81 + a22*a44*a55*a67*a86 - a22*a44*a56*a67*a85 - a22*a44*a57*a65*a86 + a22*a44*a57*a66*a85 + a22*a45*a56*a67*a84 + a22*a45*a56*a68*a83 - a22*a45*a57*a66*a84 - a22*a45*a58*a66*a83 - a22*a46*a55*a67*a84 - a22*a46*a55*a68*a83 + a22*a46*a57*a65*a84 + a22*a46*a58*a65*a83 + a22*a47*a55*a66*a84 - a22*a47*a56*a65*a84 + a22*a48*a55*a66*a83 - a22*a48*a56*a65*a83 + a23*a42*a55*a66*a88 - a23*a42*a55*a68*a86 - a23*a42*a56*a65*a88 + a23*a42*a56*a68*a85 + a23*a42*a58*a65*a86 - a23*a42*a58*a66*a85 - a23*a45*a56*a68*a82 + a23*a45*a58*a66*a82 + a23*a46*a55*a68*a82 - a23*a46*a58*a65*a82 - a23*a48*a55*a66*a82 + a23*a48*a56*a65*a82 - a24*a42*a55*a67*a86 + a24*a42*a56*a67*a85 + a24*a42*a57*a65*a86 - a24*a42*a57*a66*a85 - a24*a45*a56*a67*a82 + a24*a45*a57*a66*a82 + a24*a46*a55*a67*a82 - a24*a46*a57*a65*a82 - a24*a47*a55*a66*a82 + a24*a47*a56*a65*a82 + a11*a22*a44*a55*a66*a88 - a11*a22*a44*a55*a68*a86 - a11*a22*a44*a56*a65*a88 + a11*a22*a44*a56*a68*a85 + a11*a22*a44*a58*a65*a86 - a11*a22*a44*a58*a66*a85 - a11*a22*a45*a56*a68*a84 + a11*a22*a45*a58*a66*a84 + a11*a22*a46*a55*a68*a84 - a11*a22*a46*a58*a65*a84 - a11*a22*a48*a55*a66*a84 + a11*a22*a48*a56*a65*a84 - a11*a24*a42*a55*a66*a88 + a11*a24*a42*a55*a68*a86 + a11*a24*a42*a56*a65*a88 - a11*a24*a42*a56*a68*a85 - a11*a24*a42*a58*a65*a86 + a11*a24*a42*a58*a66*a85 + a11*a24*a45*a56*a68*a82 - a11*a24*a45*a58*a66*a82 - a11*a24*a46*a55*a68*a82 + a11*a24*a46*a58*a65*a82 + a11*a24*a48*a55*a66*a82 - a11*a24*a48*a56*a65*a82 - a12*a21*a44*a55*a66*a88 + a12*a21*a44*a55*a68*a86 + a12*a21*a44*a56*a65*a88 - a12*a21*a44*a56*a68*a85 - a12*a21*a44*a58*a65*a86 + a12*a21*a44*a58*a66*a85 + a12*a21*a45*a56*a68*a84 - a12*a21*a45*a58*a66*a84 - a12*a21*a46*a55*a68*a84 + a12*a21*a46*a58*a65*a84 + a12*a21*a48*a55*a66*a84 - a12*a21*a48*a56*a65*a84 + a12*a24*a41*a55*a66*a88 - a12*a24*a41*a55*a68*a86 - a12*a24*a41*a56*a65*a88 + a12*a24*a41*a56*a68*a85 + a12*a24*a41*a58*a65*a86 - a12*a24*a41*a58*a66*a85 - a12*a24*a45*a56*a68*a81 + a12*a24*a45*a58*a66*a81 + a12*a24*a46*a55*a68*a81 - a12*a24*a46*a58*a65*a81 - a12*a24*a48*a55*a66*a81 + a12*a24*a48*a56*a65*a81 + a14*a21*a42*a55*a66*a88 - a14*a21*a42*a55*a68*a86 - a14*a21*a42*a56*a65*a88 + a14*a21*a42*a56*a68*a85 + a14*a21*a42*a58*a65*a86 - a14*a21*a42*a58*a66*a85 - a14*a21*a45*a56*a68*a82 + a14*a21*a45*a58*a66*a82 + a14*a21*a46*a55*a68*a82 - a14*a21*a46*a58*a65*a82 - a14*a21*a48*a55*a66*a82 + a14*a21*a48*a56*a65*a82 - a14*a22*a41*a55*a66*a88 + a14*a22*a41*a55*a68*a86 + a14*a22*a41*a56*a65*a88 - a14*a22*a41*a56*a68*a85 - a14*a22*a41*a58*a65*a86 + a14*a22*a41*a58*a66*a85 + a14*a22*a45*a56*a68*a81 - a14*a22*a45*a58*a66*a81 - a14*a22*a46*a55*a68*a81 + a14*a22*a46*a58*a65*a81 + a14*a22*a48*a55*a66*a81 - a14*a22*a48*a56*a65*a81)*lambda^2 + (a11*a22*a47*a55*a83 - a11*a22*a45*a57*a83 - a11*a23*a42*a57*a85 + a11*a23*a45*a57*a82 - a11*a23*a47*a55*a82 + a12*a21*a45*a57*a83 - a12*a21*a47*a55*a83 + a12*a23*a41*a57*a85 - a12*a23*a45*a57*a81 + a12*a23*a47*a55*a81 +

a13*a21*a42*a57*a85 - a13*a21*a45*a57*a82 + a13*a21*a47*a55*a82 - a13*a22*a41*a57*a85 + a13*a22*a45*a57*a81 - a13*a22*a47*a55*a81 - a11*a22*a46*a67*a83 + a11*a22*a47*a66*a83 - a11*a23*a42*a67*a86 + a11*a23*a46*a67*a82 - a11*a23*a47*a66*a82 + a12*a21*a46*a67*a83 - a12*a21*a47*a66*a83 + a12*a23*a41*a67*a86 - a12*a23*a46*a67*a81 + a12*a23*a47*a66*a81 + a13*a21*a42*a67*a86 - a13*a21*a46*a67*a82 + a13*a21*a47*a66*a82 - a13*a22*a41*a67*a86 + a13*a22*a46*a67*a81 - a13*a22*a47*a66*a81 + a11*a45*a56*a67*a83 - a11*a45*a57*a66*a83 - a11*a46*a55*a67*a83 + a11*a46*a57*a65*a83 + a11*a47*a55*a66*a83 - a11*a47*a56*a65*a83 - a13*a41*a55*a67*a86 + a13*a41*a56*a67*a85 + a13*a41*a57*a65*a86 - a13*a41*a57*a66*a85 - a13*a45*a56*a67*a81 + a13*a45*a57*a66*a81 + a13*a46*a55*a67*a81 - a13*a46*a57*a65*a81 - a13*a47*a55*a66*a81 + a13*a47*a56*a65*a81 + a22*a45*a56*a67*a83 - a22*a45*a57*a66*a83 - a22*a46*a55*a67*a83 + a22*a46*a57*a65*a83 + a22*a47*a55*a66*a83 - a22*a47*a56*a65*a83 - a23*a42*a55*a67*a86 + a23*a42*a56*a67*a85 + a23*a42*a57*a65*a86 - a23*a42*a57*a66*a85 - a23*a45*a56*a67*a82 + a23*a45*a57*a66*a82 + a23*a46*a55*a67*a82 - a23*a46*a57*a65*a82 - a23*a47*a55*a66*a82 + a23*a47*a56*a65*a82 - a11*a22*a44*a55*a67*a86 + a11*a22*a44*a56*a67*a85 + a11*a22*a44*a57*a65*a86 - a11*a22*a44*a57*a66*a85 - a11*a22*a45*a56*a67*a84 - a11*a22*a45*a56*a68*a83 + a11*a22*a45*a57*a66*a84 + a11*a22*a45*a58*a66*a83 + a11*a22*a46*a55*a67*a84 + a11*a22*a46*a55*a68*a83 - a11*a22*a46*a57*a65*a84 - a11*a22*a46*a58*a65*a83 - a11*a22*a47*a55*a66*a84 + a11*a22*a47*a56*a65*a84 - a11*a22*a48*a55*a66*a83 + a11*a22*a48*a56*a65*a83 - a11*a23*a42*a55*a66*a88 + a11*a23*a42*a55*a68*a86 + a11*a23*a42*a56*a65*a88 - a11*a23*a42*a56*a68*a85 - a11*a23*a42*a58*a65*a86 + a11*a23*a42*a58*a66*a85 + a11*a23*a45*a56*a68*a82 - a11*a23*a45*a58*a66*a82 - a11*a23*a46*a55*a68*a82 + a11*a23*a46*a58*a65*a82 + a11*a23*a48*a55*a66*a82 - a11*a23*a48*a56*a65*a82 + a11*a24*a42*a55*a67*a86 - a11*a24*a42*a56*a67*a85 - a11*a24*a42*a57*a65*a86 + a11*a24*a42*a57*a66*a85 + a11*a24*a45*a56*a67*a82 - a11*a24*a45*a57*a66*a82 - a11*a24*a46*a55*a67*a82 + a11*a24*a46*a57*a65*a82 + a11*a24*a47*a55*a66*a82 - a11*a24*a47*a56*a65*a82 + a12*a21*a44*a55*a67*a86 - a12*a21*a44*a56*a67*a85 - a12*a21*a44*a57*a65*a86 + a12*a21*a44*a57*a66*a85 + a12*a21*a45*a56*a67*a84 + a12*a21*a45*a56*a68*a83 - a12*a21*a45*a57*a66*a84 - a12*a21*a45*a58*a66*a83 - a12*a21*a46*a55*a67*a84 - a12*a21*a46*a55*a68*a83 + a12*a21*a46*a57*a65*a84 + a12*a21*a46*a58*a65*a83 + a12*a21*a47*a55*a66*a84 - a12*a21*a47*a56*a65*a84 + a12*a21*a48*a55*a66*a83 - a12*a21*a48*a56*a65*a83 + a12*a23*a41*a55*a66*a88 - a12*a23*a41*a55*a68*a86 - a12*a23*a41*a56*a65*a88 + a12*a23*a41*a56*a68*a85 + a12*a23*a41*a58*a65*a86 - a12*a23*a41*a58*a66*a85 - a12*a23*a45*a56*a68*a81 + a12*a23*a45*a58*a66*a81 + a12*a23*a46*a55*a68*a81 - a12*a23*a46*a58*a65*a81 - a12*a23*a48*a55*a66*a81 + a12*a23*a48*a56*a65*a81 - a12*a24*a41*a55*a67*a86 + a12*a24*a41*a56*a67*a85 + a12*a24*a41*a57*a65*a86 - a12*a24*a41*a57*a66*a85 - a12*a24*a45*a56*a67*a81 +

a12*a24*a45*a57*a66*a81 + a12*a24*a46*a55*a67*a81 - a12*a24*a46*a57*a65*a81 - a12*a24*a47*a55*a66*a81 + a12*a24*a47*a56*a65*a81 + a13*a21*a42*a55*a66*a88 - a13*a21*a42*a55*a68*a86 - a13*a21*a42*a56*a65*a88 + a13*a21*a42*a56*a68*a85 + a13*a21*a42*a58*a65*a86 - a13*a21*a42*a58*a66*a85 - a13*a21*a45*a56*a68*a82 + a13*a21*a45*a58*a66*a82 + a13*a21*a46*a55*a68*a82 - a13*a21*a46*a58*a65*a82 - a13*a21*a48*a55*a66*a82 + a13*a21*a48*a56*a65*a82 - a13*a22*a41*a55*a66*a88 + a13*a22*a41*a55*a68*a86 + a13*a22*a41*a56*a65*a88 - a13*a22*a41*a56*a68*a85 - a13*a22*a41*a58*a65*a86 + a13*a22*a41*a58*a66*a85 + a13*a22*a45*a56*a68*a81 - a13*a22*a45*a58*a66*a81 - a13*a22*a46*a55*a68*a81 + a13*a22*a46*a58*a65*a81 + a13*a22*a48*a55*a66*a81 - a13*a22*a48*a56*a65*a81 - a14*a21*a42*a55*a67*a86 + a14*a21*a42*a56*a67*a85 + a14*a21*a42*a57*a65*a86 - a14*a21*a42*a57*a66*a85 - a14*a21*a45*a56*a67*a82 + a14*a21*a45*a57*a66*a82 + a14*a21*a46*a55*a67*a82 - a14*a21*a46*a57*a65*a82 - a14*a21*a47*a55*a66*a82 + a14*a21*a47*a56*a65*a82 + a14*a22*a41*a55*a67*a86 - a14*a22*a41*a56*a67*a85 - a14*a22*a41*a57*a65*a86 + a14*a22*a41*a57*a66*a85 + a14*a22*a45*a56*a67*a81 - a14*a22*a45*a57*a66*a81 - a14*a22*a46*a55*a67*a81 + a14*a22*a46*a57*a65*a81 + a14*a22*a47*a55*a66*a81 - a14*a22*a47*a56*a65*a81)*lambda + (a11*a22*a45*a57*a66*a83 - a11*a22*a45*a56*a67*a83 + a11*a22*a46*a55*a67*a83 - a11*a22*a46*a57*a65*a83 - a11*a22*a47*a55*a66*a83 + a11*a22*a47*a56*a65*a83 + a11*a23*a42*a55*a67*a86 - a11*a23*a42*a56*a67*a85 - a11*a23*a42*a57*a65*a86 + a11*a23*a42*a57*a66*a85 + a11*a23*a45*a56*a67*a82 - a11*a23*a45*a57*a66*a82 - a11*a23*a46*a55*a67*a82 + a11*a23*a46*a57*a65*a82 + a11*a23*a47*a55*a66*a82 - a11*a23*a47*a56*a65*a82 + a12*a21*a45*a56*a67*a83 - a12*a21*a45*a57*a66*a83 - a12*a21*a46*a55*a67*a83 + a12*a21*a46*a57*a65*a83 + a12*a21*a47*a55*a66*a83 - a12*a21*a47*a56*a65*a83 - a12*a23*a41*a55*a67*a86 + a12*a23*a41*a56*a67*a85 + a12*a23*a41*a57*a65*a86 - a12*a23*a41*a57*a66*a85 - a12*a23*a45*a56*a67*a81 + a12*a23*a45*a57*a66*a81 + a12*a23*a46*a55*a67*a81 - a12*a23*a46*a57*a65*a81 - a12*a23*a47*a55*a66*a81 + a12*a23*a47*a56*a65*a81 - a13*a21*a42*a55*a67*a86 + a13*a21*a42*a56*a67*a85 + a13*a21*a42*a57*a65*a86 - a13*a21*a42*a57*a66*a85 - a13*a21*a45*a56*a67*a82 + a13*a21*a45*a57*a66*a82 + a13*a21*a46*a55*a67*a82 - a13*a21*a46*a57*a65*a82 - a13*a21*a47*a55*a66*a82 + a13*a21*a47*a56*a65*a82 + a13*a22*a41*a55*a67*a86 - a13*a22*a41*a56*a67*a85 - a13*a22*a41*a57*a65*a86 + a13*a22*a41*a57*a66*a85 + a13*a22*a45*a56*a67*a81 - a13*a22*a45*a57*a66*a81 - a13*a22*a46*a55*a67*a81 + a13*a22*a46*a57*a65*a81 + a13*a22*a47*a55*a66*a81 - a13*a22*a47*a56*a65*a81)